

Ferromagnetic Resonance in Thin Films. I. Theory of Normal-Mode Frequencies

M. SPARKS*

Science Center, North American Rockwell Corporation, Thousand Oaks, California 91360

(Received 28 July 1969)

A theory is developed for the frequencies of the general ferromagnetic normal modes of a sample of arbitrary shape and size with both exchange and demagnetization energies included. The frequencies of the modes of rectangular and circular films are calculated by casting the linearized equation of motion of the magnetization into the form of an eigenvalue equation, which is solved by a variational method. The results explain the experiments of Dillon, Besser, Sparks *et al.*, Freedman and Brundle, and Voltmer in detail qualitatively and typically to within $\sim 5\text{--}10\%$ quantitatively for the mode spacings, with possible exceptions for the first few low-order modes in some samples, for which several contributions to the line spacings are difficult to estimate accurately. Pinning the surface spins has little effect on the frequencies and intensities of magnetostatic modes (with negligible exchange energy). The theory has implications concerning the main-resonance position in finite films, and together with experiments, further verifies Portis's mode-spacing theory. A simple physical explanation of the results is given, and the relation of the results for finite films to those for infinite films is given.

1. INTRODUCTION

IN this first paper of a series on ferromagnetic resonance in thin films and disks, a theory is developed for the frequencies of the ferromagnetic normal modes of these systems. In Paper II, the linewidths of the modes will be calculated, and in Paper III, a theory of pinning¹ will be presented. The effect of an inhomogeneous internal field H_i and saturation magnetization M_s on the frequencies of high-order modes and a source of the inhomogeneous H_i and M_s will be considered in Paper IV. Experimental results will be presented and discussed in Paper V by P. Besser and M. Sparks.

The normal modes of an infinite ferromagnetic system are ordinary spin waves having magnetization

$$\mathbf{M} = M_s \hat{z} + \mathbf{m}, \quad (1)$$

where \hat{z} is a unit vector along the z axis and the small transverse microwave component \mathbf{m} is a plane wave: $\mathbf{m} \propto \exp(i\mathbf{k} \cdot \mathbf{r})$. For a finite sample, spin waves with wavelengths $\lambda = 2\pi/k$ short with respect to the sample dimensions can be used as approximate normal modes, but the approximation is poor when λ is not small with respect to the sample dimensions. The function $\mathbf{m}(\mathbf{r})$ is then determined by the size and shape of the sample. When the exchange energy is negligible, as it is for slow variations of \mathbf{m} as a function of \mathbf{r} , these modes are called *magnetostatic modes*. When the microwave demagnetization energy is negligible, the modes will be called *exchange modes*. In both cases it is assumed that the sample is sufficiently small that electromagnetic propagation is negligible.

Very briefly, the state of the theoretical and experimental results for magnetostatic and exchange modes prior to the present series of papers and that of Sparks *et al.*² was the following: Only exchange modes had been observed in metallic films,³ the linewidths being too

large for the magnetostatic modes to be resolved. The frequencies of the exchange modes were fairly well understood in terms of the theories of Kittel,⁴ Wigen, Kooi, and co-workers,³ and Portis,⁵ but the intensities were not understood.

Only magnetostatic modes had been observed in thin disks of ferromagnetic insulators since the disks were far too thick for the exchange modes to be resolved. Dillon⁶ had explained his observation of magnetostatic modes in thin disks of yttrium iron garnet (YIG) and manganese ferrite in terms of Walker's theory⁷ for the modes in spheroids. The major difficulty with the interpretation was that the theoretical values of the mode intensities were zero except for the Kittel uniform-precession mode, whereas many strongly excited modes were observed. As a result of the recent success of Mee and co-workers⁸ in growing single-crystal YIG films having linewidths $\Delta H \cong 1$ Oe, the magnetostatic, exchange, and mixed modes can be observed in a single thin film. No theories existed for the frequencies or intensities of these modes in finite films.

White and Solt,⁹ Dillon,⁶ and others had studied the magnetostatic modes experimentally. Walker⁷ calculated the frequencies of the magnetostatic modes in a spheroid, and Fletcher and Kittel,¹⁰ Damon and Eshbach,¹¹ and Akhiezer and co-workers¹² extended the cal-

20, 450 (1968). These two references should lead the reader into the vast literature on ferromagnetic resonance in thin metallic films.

⁴ C. Kittel, Phys. Rev. **110**, 1295 (1958).

⁵ A. M. Portis, Appl. Phys. Letters **2**, 69 (1963).

⁶ J. F. Dillon, J. Appl. Phys. **31**, 1605 (1960); Bull. Am. Phys. Soc. **1**, 125 (1956).

⁷ L. R. Walker, Phys. Rev. **105**, 390 (1957).

⁸ J. E. Mee, J. L. Archer, R. H. Meade, and T. N. Hamilton, Appl. Phys. Letters **10**, 289 (1967); J. E. Mee, IEEE Trans. MAG-3, 190 (1967).

⁹ R. L. White and I. H. Solt, Phys. Rev. **104**, 56 (1956).

¹⁰ P. C. Fletcher and C. Kittel, Phys. Rev. **120**, 2004 (1960).

¹¹ R. W. Damon and J. R. Eshbach, J. Phys. Chem. Solids **19**, 308 (1961).

¹² A. I. Akhiezer, V. G. Bar'Yakhtar, and S. V. Peletimskii, *Spin Waves* (North-Holland Publishing Co., Amsterdam, 1968); also see M. Sparks (unpublished).

* Present address: The RAND Corp., Santa Monica, Calif.

¹ See the discussion of pinning in Sec. 2.

² M. Sparks, B. R. Tittmann, J. E. Mee, and C. Newkirk, J. Appl. Phys. **40**, 1518 (1969).

³ P. E. Wigen, C. F. Kooi, M. R. Shanabarger, and Thomas C. Rossing, Phys. Rev. Letters **9**, 206 (1962); C. F. Kooi, *ibid.*

culations to an infinite circular cylinder, an infinite film (infinite in two directions, but having a finite thickness) in parallel resonance,¹³ and an infinite film in perpendicular resonance, respectively. Gann¹⁴ and others¹⁴ had included exchange and demagnetization energies in studies of the long-wavelength modes in infinite films. Many investigators had studied exchange modes in metallic films.³

In the present paper a theory is developed for the frequencies of the general ferromagnetic normal modes of a sample of arbitrary size and shape with both demagnetization and exchange energies included. Detailed calculations are given for the frequencies of the modes of rectangular and circular films, both thin and thick. For the case of no explicit pinning of the spins on the surface of a rectangular film, the present results are simply related to those of an infinite film in perpendicular and in parallel resonance (where the infinite-film results are known). The infinite-film results therefore can be used to visualize the results for finite films (Secs. 5 and 9). A simple physical model which explains the result intuitively is given in Sec. 7.

The theoretical results for the frequencies explain qualitatively the detailed experimental observations by Besser,¹⁵ Dillon,⁶ Sparks *et al.*,² Brundle and Freedman,¹⁶ and Voltmer¹⁶ of the ferromagnetic-resonance frequencies in thin and thick films and disks. Quantitatively, the calculated spacings between modes agree with the small amount of existing experimental data for thick films (thickness $S \gtrsim 3 \mu$) within ~ 5 – 10% , with possible exceptions for the first few spacing of the low-order modes, as discussed in Sec. 4. The qualitative features of the results for thin films ($S \lesssim 3 \mu$) are explained by the theory,² but the quantitative agreement for thin films of YIG is not expected to be good because the variation of H_i across the thickness of the film may be rather large, and the functional form of H_i is unknown.

According to Portis's theory⁵ of the low-order exchange modes, \mathbf{m} is large only in the interior of the film, rather than extending across the full thickness. This was verified by measurements² of the magnetostatic splitting of the first exchange mode in a film $\sim 1 \mu$ thick, which were interpreted according to the present theory. The spacing of these magnetostatic modes corresponded to a thickness approximately one-half as large as that obtained from optical measurements and from the spacing of the high-order modes. Nonzero slopes of the disper-

sion curves of the even, higher-order modes (Fig. 13) observed by Besser¹⁵ are further evidence for Portis-type modes.

It is well known that the frequency of the main-resonance mode in a finite film is shifted slightly from that of the Kittel uniform-precession mode ($\mathbf{k}=0$) in an infinite film. The present theory indicates that this shift is a consequence of the *microwave* demagnetization field (giving the ω_d term to be discussed in detail) and a shift in the weighted average of the *static* internal field H_i . See Sec. 6. Other factors such as anisotropy, strain, etc., could also effect the shift, of course.

The normal modes are quite sensitive to slight changes in the sample shape. This was demonstrated dramatically by Dillon⁶ in experiments in which one or both surfaces of a circular disk were ground to form plano-convex or double-convex samples. Both of these samples showed one large resonance line and three or four smaller lines, in contrast to a series of 27 distinguishable lines in a well-defined series observed in a double-plano sample. The plano-convex and double-convex samples resemble a spheroid, for which only one mode—the uniform precession—is excited by a uniform microwave field. For the double-plano sample, formally quantizing the radial wave vector in the infinite-circular-film results gives a series of modes with large intensities, as observed. See the Appendix and Sec. 8. The two sets of \mathbf{m} for the spheroid and the circular disk are quite different. For one set of modes in a spheroid, $\mathbf{m} \sim \rho^n e^{in\phi}$ for the n th mode, where $\rho^2 \equiv x^2 + y^2$ and $\phi \equiv \tan^{-1}(y/x)$. The most closely corresponding modes for the circular disk have $\mathbf{m} \sim J_n(k_\rho \rho) e^{in\phi} \cos k_z z$, where $k_\rho r_0$ is the first zero of J_n and $0 < k_z < \pi/S$.

Similarly, the eigenfunction \mathbf{m} and intensities for a long rectangular cylinder are expected to be drastically different from those of a long ellipsoidal cylinder. Thus the suggestion of Wolfram and De Wames¹⁴ that the eigenvectors for a "flat ellipse are possibly more realistic than the plane-wave solutions . . ." for double-plano samples is untenable. Wolfram and De Wames also concluded that in finite samples, such as circular and rectangular films, the main-resonance mode should be the uniform precession and that previous considerations of pinning^{4,2} were incorrect. Their conclusions were based on the fact that the pure magnetostatic modes (exchange constant $D=0$ and no pinning mechanism) in an infinite elliptical cylinder magnetized along its axis had large precession amplitudes at the surface of the cylinder. (This is true also for the case of a spheroidal sample.⁷) The conclusions are incorrect because no pinning mechanism was included in their model calculation and the uniform-precession microwave demagnetization field and the internal field are constant throughout the infinite elliptical cylinder. It is easy to show by direct substitution into the equations of motion (6) that the uniform precession is not a normal mode of a finite disk or film, a result which is not surprising since

¹³ Perpendicular (or parallel) resonance indicates that the applied field \mathbf{H}_{app} is perpendicular (or parallel) to the plane of the film.

¹⁴ V. V. Gann, *Soviet Phys.—Solid State* **8**, 2537 (1967); P. H. Carr, A. J. Slobodnik, and James C. Sethares, 1969 International Microwave Symposium, Dallas, Texas (unpublished); T. Wolfram and R. E. De Wames (unpublished).

¹⁵ P. Besser (private communication). Also see Paper V of the present series.

¹⁶ L. K. Brundle and N. J. Freedman, *Electron. Letters* **4**, 132 (1968). Similar experiments on both surface and bulk modes have been carried out by F. Voltmer (unpublished).

the internal field and the microwave demagnetization field are quite inhomogeneous near the edges of the disk or film, thus making the precession amplitudes small there since the edge spins are off resonance, roughly speaking. The direct optical observation of magnetostatic modes by Dillon and co-workers^{16a} shows directly that the uniform precession is not a normal mode of a finite disk.

2. PINNING OF SURFACE SPINS

The common concept of surface-spin pinning is the following: The variation of the transverse magnetization m across the thickness of the film is described by a single cosinusoidal function

$$m = m_0 \cos k_z z'$$

(for the even modes), where the z' axis is perpendicular to the plane of the film. The *pinning conditions* which m satisfies at the surfaces of the film are assumed to be

$$am + b \frac{dm}{dz'} = 0.$$

The surface spins are said to be *pinned* if $b=0$, or *unpinned* if $a=0$.

Even though this concept of pinning can be quite useful, it should be emphasized that there are cases in which it can cause confusion. First of all, the true boundary conditions are those which the potential satisfies at $z' = \pm \infty$. The fields must satisfy continuity conditions at the sample surfaces, but the problem of determining m and the normal-mode frequencies cannot be solved as a problem with fixed boundary conditions on m at the film surfaces. Thus the name "pinning condition," rather than boundary condition, was used above.

Mathematically, for the magnetostatic-mode problem ($D=0$), specifying the usual electromagnet "boundary conditions" (the vanishing of the potential at infinity and the continuity of normal \mathbf{B} and tangential \mathbf{H}) determine the solutions to (2) and (3). For the exchange-mode problem [$\mathbf{h}=0$ in (2)], specifying a pinning condition at each surface of an infinite film determines the solutions. With both \mathbf{h} and D included, specifying both the electromagnetic boundary conditions and the pinning conditions at each surface determines the solutions. See Sec. 9.

Second, it is now apparent that in most thin films the surface of the film cannot be considered as a mathematical plane, but must be considered as a region of finite thickness ϵ .¹⁷ For the large- k_z modes having wavelengths approaching ϵ the variation of m in the surface

^{16a} J. F. Dillon, Jr., L. R. Walker, and J. P. Remeika, in *Proceedings of the International Conference of Magnetism, Nottingham, 1964* (The Institute of Physics and The Physical Society, London, 1965), pp. 369-373.

¹⁷ M. Sparks, Phys. Rev. Letters 22, 1111 (1969). See also III of the present series: M. Sparks, second following paper, Phys. Rev. B 1, 3869 (1970).

layer becomes important in determining both the intensities and frequencies of the modes, and the concept of a sharp mathematical boundary surface becomes meaningless. In the present paper, only the case of a perfectly sharp surface is considered. Effects of a surface layer of nonzero thickness are considered in subsequent papers in the present series. Third, for an inhomogeneous internal field, m does not vary cosinusoidally, and the concept of a constant wave vector k_z loses meaning.

Finally, it is easy to show that the single cosine function considered above is not a solution to (6) when both exchange and demagnetization energies are included. In particular, Benson and Mills¹⁸ suggested that a rounding of m near the surface to make $dm/dz' = 0$ at the surface is important in some cases. For example, consider a wave of the form

$$m = m_0 \{ \cos \pi z' - (\pi/k_r) \exp[-k_r(z' + \frac{1}{2}S)] \},$$

where S is the film thickness. If $k_r \gg \pi$, then over most of the volume of the sample $m \cong m_0 \cos \pi z'$, which is a pinned mode. But the small decaying exponential term rounds off m near the surface at $z' = -\frac{1}{2}S$ and makes $dm/dz' = 0$ at $z' = -\frac{1}{2}S$, which is the unpinned condition. The point is that specifying the degree of pinning at the surfaces determines m everywhere when m is a single cosinusoidal function, but not when it is the sum of more than one function.

Fortunately, a large number of ferromagnetic-resonance experiments in thin films can be explained in terms of a single cosinusoidal or single decaying-exponential function. However, this is not the case in general, especially where intensities are concerned, and it is important to distinguish between *pinned modes* and modes with *pinned intensities*. The former have $m=0$ at the surfaces, and the latter have intensities corresponding to single cosinusoidal functions with $m=0$ at the surfaces. This will be discussed further in Sec. 9.

3. VARIATIONAL EXPRESSION FOR FREQUENCIES

The equation of motion of the magnetization \mathbf{M} is

$$\frac{d\mathbf{M}}{dt} = -|\gamma| \mathbf{M} \times \mathbf{H}, \quad (2)$$

where \mathbf{M} is given by (1), $\mathbf{H} = H_i \hat{z} + \mathbf{h} + \Delta \nabla^2 \mathbf{M}$ is the total effective field, \hat{z} is a unit vector along the z axis, Δ is the exchange constant, $H_i = H_{\text{app}} - 4\pi N_z M_z$ is the internal field, H_{app} is the applied field, and N_z is the demagnetization factor for the z axis. The microwave demagnetization field \mathbf{h} is determined by the relations

$$\nabla \cdot \mathbf{b} = \nabla \cdot (\mathbf{h} + 4\pi \mathbf{m}) = 0, \quad \nabla \times \mathbf{h} = 0. \quad (3)$$

Walker⁷ and others¹⁰⁻¹² studied magnetostatic modes by

¹⁸ H. Benson and D. L. Mills, Phys. Rev. 188, 849 (1969).

solving these equations with no exchange ($\Lambda=0$) by eliminating \mathbf{m} and solving the potential problem for ψ , where $\mathbf{h}=\nabla\psi$. By eliminating \mathbf{h} rather than \mathbf{m} we obtain an eigenvalue equation, which is solved by a variational method. The eigenvalue equation can be obtained from (2) and (3) as follows: Linearizing (2) by setting M_x equal to the saturation magnetization M_s , dropping the small terms $\mathbf{m}\times\mathbf{h}$ and $\mathbf{m}\times\Lambda\nabla^2\mathbf{m}$, and assuming $\exp(i\omega t)$ time dependence gives

$$\begin{aligned} -ih_y + (\bar{H}_i - \Lambda\nabla^2)im_y &= \bar{\Omega}m_x, \\ -h_x + (\bar{H}_i - \Lambda\nabla^2)m_x &= i\bar{\Omega}m_y, \end{aligned} \quad (4)$$

where $\bar{H}_i \equiv H_i/M_s$ and $\bar{\Omega} = \omega/|\gamma|M_s$. The demagnetization field \mathbf{h} can be eliminated from (4) by setting $\mathbf{h}=\nabla\psi$. This reduces (3) to $-\nabla^2\psi=4\pi\nabla\cdot\mathbf{m}$, whose infinite-space Green's-function solution is $\psi = \mathcal{G}\nabla\cdot\mathbf{m}$, where the Green's operator \mathcal{G} is defined as

$$\mathcal{G}f(\mathbf{r}) \equiv \int_{\text{all space}} d\mathbf{r}_1 \frac{1}{|\mathbf{r}-\mathbf{r}_1|} f(\mathbf{r}_1). \quad (5)$$

Substituting $\mathbf{h}=\nabla\mathcal{G}\nabla\cdot\mathbf{m}$ into (4) and writing the results in terms of the circular variables, $m^\pm \equiv m_x \pm im_y$, gives the eigenvalue equation

$$\begin{aligned} \left[\begin{array}{cc} \bar{H}_i - \Lambda\nabla^2 - \frac{1}{2}\partial^+\mathcal{G}\partial^- & -\frac{1}{2}\partial^+\mathcal{G}\partial^+ \\ \frac{1}{2}\partial^-\mathcal{G}\partial^- & -\bar{H}_i + \Lambda\nabla^2 + \frac{1}{2}\partial^-\mathcal{G}\partial^+ \end{array} \right] \begin{bmatrix} m^+ \\ m^- \end{bmatrix} \\ = \bar{\Omega} \begin{bmatrix} m^+ \\ m^- \end{bmatrix}, \end{aligned} \quad (6)$$

where $\partial^\pm \equiv \partial/\partial x \pm i\partial/\partial y$. It was verified that spin waves, the lowest-order magnetostatic modes in a sphere, and all of the magnetostatic modes in infinite films in both parallel and perpendicular resonance are solutions of (6).

The δ functions in the demagnetization terms $\partial^\pm m^\pm$ resulting from the discontinuities of m^\pm at the surfaces of the sample give rise to integrals over the surfaces. These surface terms will not be considered explicitly since it is easier to use an integration by parts and treat the surface sources and bulk sources together. The δ functions and derivatives of δ function at the surface from the exchange term $\nabla^2 m^\pm$ are dropped. The effect of exchange on the surface spins is discussed in Sec. 6 and in Ref. 17. The present variational method allows us to study the effect of this and other pinning mechanisms, as discussed in Sec. 9.

The general eigenvalue equation (6) for the frequencies of the normal modes can be simplified by dropping the off-diagonal terms (which couple m^+ and m^-) in the matrix operator, which is equivalent to neglecting the third Holstein-Primakoff transformation^{19,20} for ordinary spin waves. This gives the circular-

precession-approximation²¹ result

$$(\bar{H}_i - \Lambda\nabla^2 - \frac{1}{2}\partial^+\mathcal{G}\partial^-)m^+ = \bar{\Omega}m^+. \quad (7)$$

The circular-precession approximation is discussed in Sec. 6. Benson and Mills¹⁸ have carried out a variational calculation without neglecting the off-diagonal matrix elements in considering the effects of exchange on the Damon and Eshbach¹¹ surface waves.

Since the operator in (7) is Hermitian, the normalized diagonal matrix element $\bar{\Omega}_n$ is a variational expression for the n th eigenvalue Ω_n :

$$\Omega_n \cong \bar{\Omega}_n \equiv \langle \bar{H}_i - \Lambda\nabla^2 - \frac{1}{2}\partial^+\mathcal{G}\partial^- \rangle, \quad (8)$$

where the average $\langle \mathcal{L} \rangle$ of any operator \mathcal{L} is defined as

$$\langle \mathcal{L} \rangle \equiv \int_{\text{sample}} d\mathbf{r} (\tilde{m}_n^+)^* \mathcal{L} \tilde{m}_n^+ / \int_{\text{sample}} d\mathbf{r} |\tilde{m}_n^+|^2, \quad (9)$$

where * denotes the complex conjugate. Since (8) is a variational expression, $\bar{\Omega}_n$ will be a very good approximation to Ω_n if the trial function \tilde{m}_n^+ is a fairly good approximation to the true m_n^+ ; i.e., if $\tilde{m}_n^+ = m_n^+ + \nu f$, where $\nu \ll 1$, then $\bar{\Omega}_n = \Omega_n + O(\nu^2)$, where $O(\nu^2)$ is of the order of ν^2 .

The general result (8) can be written as

$$\bar{\omega}_n = |\gamma| \langle H_i \rangle + \omega_{\text{exo}} + \omega_d, \quad (10)$$

where

$$\omega_{\text{exo}} \equiv |\gamma| M_s \langle \Lambda\nabla^2 \rangle \quad (11)$$

and

$$\begin{aligned} \omega_d &\equiv -\frac{1}{2} |\gamma| M_s \langle \partial^+\mathcal{G}\partial^- \rangle \\ &= -\frac{1}{2} |\gamma| M_s \int_{\text{sample}} d\mathbf{r} \tilde{m}_n^+(\mathbf{r})^* \int_{\text{all space}} d\mathbf{r}_1 \partial^+ \frac{1}{|\mathbf{r}-\mathbf{r}_1|} \\ &\quad \times \partial_1^- \tilde{m}_n^+(\mathbf{r}_1) / \int_{\text{sample}} d\mathbf{r} |\tilde{m}_n^+|^2 \end{aligned} \quad (12)$$

with $\partial_1^- \equiv (\partial/\partial x_1) - i(\partial/\partial y_1)$. Equation (12) can be simplified by integrating the \mathbf{r}_1 integral by parts and using

$$\frac{1}{|\mathbf{r}-\mathbf{r}_1|} = \frac{1}{2\pi^2} \int_{\text{all space}} d\mathbf{q} \frac{e^{i\mathbf{q}\cdot(\mathbf{r}_1-\mathbf{r})}}{q^2}. \quad (13)$$

This gives

$$\begin{aligned} \omega_d &= \frac{|\gamma| M_s}{4\pi^2} \int_{\text{all space}} d\mathbf{q} \frac{q_x^2}{q^2} \left| \int_{\text{sample}} d\mathbf{r} \tilde{m}_n^+ e^{i\mathbf{q}\cdot\mathbf{r}} \right|^2 / \\ &\quad \int_{\text{sample}} d\mathbf{r} |\tilde{m}_n^+|^2, \end{aligned} \quad (14)$$

where $q_i^2 = q_x^2 + q_y^2$. The approximations made in obtaining this general result were the linearization of the equations of motion, the circular precession approxima-

¹⁹ T. Holstein and H. Primakoff, Phys. Rev. **58**, 1098 (1940).

²⁰ M. Sparks, *Ferromagnetic Relaxation Theory* (McGraw-Hill Book Co., New York, 1964).

²¹ See Sec. 3.3 and p. 69 of Sparks (Ref. 20).

tion, and the variational characterization of the eigenvalues.

In Sec. 4, the variational characterization (10) of the eigenvalues will be used in a very simple way to obtain the first-order approximation to the normal-mode frequencies. Simple trial functions containing no adjustable parameters are used. The choice of the trial functions is motivated by physical intuition, by general considerations of the number of nodes in the function, by analogy with infinite film results, and by the fact that the solution should be a standing-type wave rather than a travelling-type wave.

It should be mentioned that the general results of the present section can be used as the starting point in more sophisticated analyses. See the reference by Benson and Mills for several examples.¹⁸ Care should be exercised in calculations involving adjustable parameters. For example, for $\Lambda=0$ the main-resonance mode is not the mode having the lowest value of ω . Thus the best function in a class of trial functions cannot be obtained by adjusting the parameters in the trial function to minimize $\tilde{\omega}_n$ in general. As another example, the best function in the set

$$m = \cos(n-p)\pi/S$$

cannot be obtained by setting $d\tilde{\omega}_n/dp=0$ with $\tilde{\omega}_n$ given by (10). This is because sources of the surface spin pinning, such as an inhomogeneous M_z , have not been included in deriving (10), and these sources, rather than $d\tilde{\omega}_n/dp=0$, will determine the value of p .

Other standard precautions for variational characterizations of eigenvalues should be observed. For example, care must be exercised in the selection of the trial functions. The choice of the trial functions was discussed in

the two previous paragraphs. As an example of a difficulty which could arise, in perpendicular resonance m^+ could be chosen as $\sim \exp(-k_z z)$, corresponding to a surface mode. However, the infinite-film¹² and infinite-cylinder¹⁰ results for magnetostatic modes indicate that if surface modes exist they are more likely to be associated with the small edge of the sample than with the large face.

4. FREQUENCIES FOR RECTANGULAR FILMS

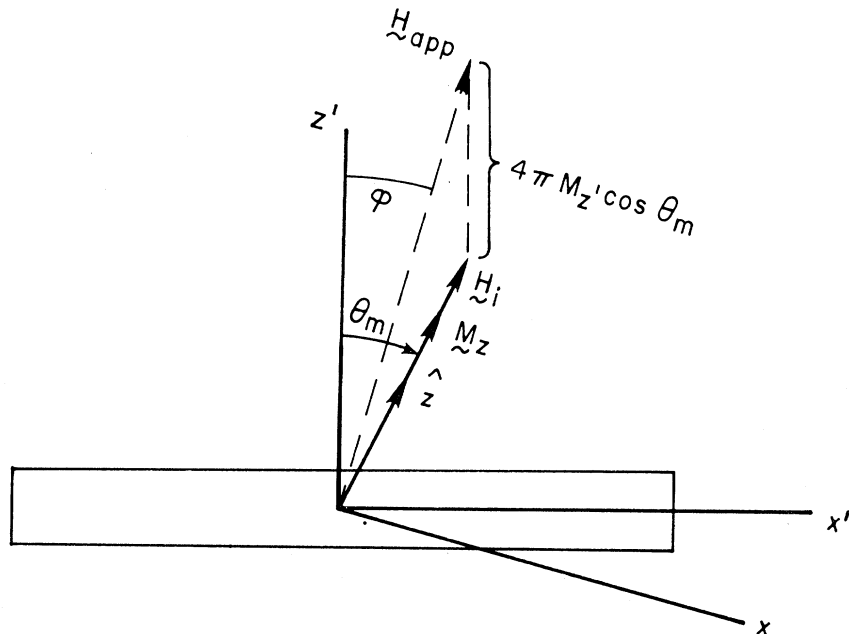
Consider a thin rectangular film having width W along the x' axis, length L along the y' axis, and thickness S along the z' axis. Since the normal modes are expected to have 0, 1, 2, ... nodes along the x' , y' , and z' axes, and m^+ is sinusoidal for an infinite film, and we want standing waves for a finite film, we choose the trial function in (8)-(14) as

$$\tilde{m}_n^+ = m_0 \cos(k_{x'} x' - \frac{1}{2} \eta_{x'} \pi) \cos(k_{y'} y' - \frac{1}{2} \eta_{y'} \pi) \times \cos(k_{z'} z' - \frac{1}{2} \eta_{z'} \pi), \quad (15)$$

where $\eta=0$ or 1 for modes even or odd in x' , y' , or z' . Note that z' is normal to the plane of the film and z is along the equilibrium position of \mathbf{M} , as illustrated in Fig. 1.

The values of the k 's are chosen to give the appropriate number of nodes. It is assumed that the spins are pinned at the edges of the sample (at $x' = \pm \frac{1}{2}W$ and $y' = \pm \frac{1}{2}L$); thus $k_{x'} = n_W \pi / W$ and $n_{y'} = N_L \pi / L$, where $n_W, n_L = 1, 2, 3 \dots$. The optical observation of magnetostatic modes by Dillon and coworkers^{16a} and the observations^{6,2,15,16} of large numbers of intense resonance modes indicate that this assumption gives better agreement with experiment than does the assumption that

FIG. 1. Schematic illustration showing fields, angles, and coordinate systems used in the text. The axis of quantization is z , and the z' axis is normal to the film surface.



$d\mathbf{m}/dz'=0$ at the small edges. Theoretically, it is expected that \mathbf{m} will be small near the small edges because the static and microwave demagnetization fields there will be different from those in the bulk of the sample away from the edges. Thus these edge spins are off resonance, roughly speaking. This is analogous to the Wigen-Kooi-type^{3,17} and Portis-type^{5,17} pinning of \mathbf{m} along the z' direction.

The intensities depend on the form of m_n^+ as well as the pinning, as discussed in Sec. 2. For the higher-order modes (large values of n_W and n_L) the assumed sinusoidal variation is expected to be fairly accurate over a large fraction of the sample volume, by analogy with the results for an infinite film. For the low-order modes, the deviation of m_n^+ from the assumed form probably is not small. The resulting deviation in the frequency is reduced by the variational characterization of the eigenfrequencies, as already mentioned. The values of $k_{z'}$ for arbitrary pinning at $z'=\pm\frac{1}{2}S$ are

$$k_{z'} = (n_S - p)\pi/S, \quad (16)$$

where $n_S=1, 2, 3, \dots$ and p ranges from 0 (pinned) to 1 (unpinned). The calculations will be carried out for *pinned modes* ($p=0$ and $m^+\sim\cos\pi/S, \sin 2\pi/S, \cos 3\pi/S, \dots$) and for *unpinned modes*²² ($p=1$ and $m^+\sim 1, \sin\pi/S, \cos 2\pi/S, \sin 3\pi/S, \dots$). Comparing the two results with experimental results gives information about pinning, as discussed in Sec. 9.

Substituting (15) into (11) gives

$$\omega_{\text{exc}} = |\gamma| D k^2, \quad (17)$$

where $k^2 \equiv k_{x'}^2 + k_{y'}^2 + k_{z'}^2$ and $D = \Delta M_s$. This result and the value of $\langle \bar{H}_i \rangle$ will be discussed in Sec. 6. Substituting (15) and (14) and evaluating the integrals over \mathbf{r} gives

$$\omega_d = \frac{|\gamma| M_s S W L}{4\pi^2 I_{z'}} \int_{\text{all space}} \frac{dq_i^2}{q^2} G_{x'} G_{y'} G_{z'}, \quad (18)$$

where

$$I_{z'} \equiv \frac{2}{S} \int_{-S/2}^{S/2} dz' \cos^2 k_{z'} z',$$

$$G_j \equiv \frac{1}{2} \left(\frac{\sin \frac{1}{2}(q_j - k_j)L_j}{\frac{1}{2}(q_j - k_j)L_j} + \frac{(-1)^{n_j} \sin \frac{1}{2}(q_j + k_j)L_j}{\frac{1}{2}(q_j + k_j)L_j} \right), \quad (19)$$

for $j=x', y', z'$, and $L_{x'}=W, L_{y'}=L$, and $L_{z'}=S$. The factor of $q_i^2 = q_x^2 + q_y^2$ in (18) can be written in the primed basis as $q_i^2 \equiv q_\theta^2 - 2q_{x'}q_{y'} \cos\theta_m \sin\theta_m$, where $q_\theta^2 \equiv q_{y'}^2 + q_{x'}^2 \cos^2\theta_m + q_{z'}^2 \sin^2\theta_m$ and θ_m is the angle between \mathbf{M}_s and the normal to the film surface, as illustrated in Fig. 1. By using this expression for q_i^2 and the fact that G_j is an even function of q_j , (18) can be reduced to

$$\omega_d = \frac{|\gamma| M_s S W L}{4\pi^2 I_{z'}} \int_{\text{all space}} \frac{dq_\theta^2}{q^2} G_{x'} G_{y'} G_{z'}. \quad (20)$$

²² Note that "pinned modes" and "unpinned modes" refer to the pinning of the spins at the large surfaces of the films at $z'=\pm\frac{1}{2}S$. For both the pinned and unpinned modes, the spins are pinned at the small edges of the film at $x'=\pm\frac{1}{2}W$ and $y'=\pm\frac{1}{2}L$.

Writing the terms in (19) gives

$$G_{x'} = \frac{1}{2} F\left[\frac{1}{2}(q_{x'} - k_{x'})W\right] + \frac{1}{2} F\left[\frac{1}{2}(q_{x'} + k_{x'})W\right] + \text{cross terms}, \quad (21)$$

where $F(\xi) \equiv \sin^2\xi/\xi^2$. By sketching G and F it is easy to see that neglecting the cross terms in $G_{x'}$ and $G_{y'}$ gives $\sim 10\%$ error for $k_{x'}=\pi/W$ and less for higher values of $k_{x'}$. Neglecting these cross terms and using the fact that the integrand in (20) is even in $q_{x'}$ and in $q_{y'}$ reduces (20) to

$$\omega_d = \frac{|\gamma| M_s S W L}{4\pi^2 I_{z'}} \int_{\text{all space}} \frac{dq_\theta^2}{q^2} F\left[\frac{1}{2}(q_{x'} - k_{x'})W\right] \times F\left[\frac{1}{2}(q_{y'} - k_{y'})L\right] G_{z'}. \quad (22)$$

In evaluating the integrals in (22) for the unpinned modes, first consider the modes with $k_{z'}=\eta_{z'}=0$. The value of $I_{z'}$ is 2, and the definition of $G_{z'}$ gives $G_{z'}=2F(\frac{1}{2}q_{z'}S)$. Approximating $F(\xi) \equiv \sin^2\xi/\xi^2$ in the $q_{x'}$ and $q_{y'}$ integrals by

$$F(\xi) \cong 1, \quad \text{for } |\xi| < \frac{1}{2}\pi \\ \cong 0, \quad \text{for } |\xi| > \frac{1}{2}\pi \quad (23)$$

reduces (22) to

$$\omega_d = \frac{|\gamma| M_s S W L}{4\pi^2} \int_Q \frac{dq_\theta^2 \sin^2 \frac{1}{2} q_{z'} S}{q^2 (\frac{1}{2} q_{z'} S)^2}, \quad (24)$$

where the volume Q is defined by $|q_{x'} - k_{x'}| < \pi/W$ and $|q_{y'} - k_{y'}| < \pi/L$, as illustrated in Fig. 2. Using $dq = (2\pi/W)(2\pi/L)dq_{z'}$ and replacing $q_{x'}^2$ and $q_{y'}^2$ by their values $k_{x'}^2$ and $k_{y'}^2$ at the center of dq , as illustrated in Fig. 2, gives

$$\omega_d \cong |\gamma| M_s S \int_{-\infty}^{\infty} \frac{dq_{z'} \frac{k_{y'}^2 + k_{x'}^2 \cos^2\theta_m + q_{z'}^2 \sin^2\theta_m}{q_{z'}^2 + k_f^2}}{\frac{\sin^2 \frac{1}{2} q_{z'} S}{(\frac{1}{2} q_{z'} S)^2}}, \quad (25)$$

where $k_f^2 \equiv k_{x'}^2 + k_{y'}^2$ is the square of wave vector in the plane of the film. Evaluating the integrals gives one of our central results:

$$\omega_d \cong 2\pi |\gamma| M_s \sin^2\theta_m + 2\pi |\gamma| M_s (\cos^2\theta_m - \cos^2\phi' \sin^2\theta_m) \times \left[1 - \frac{1}{k_f S} (1 - e^{-k_f S}) \right], \quad \text{for } m^+(z') \cong 1 \quad (26)$$

where $\cos^2\phi' \equiv k_{x'}^2/(k_{x'}^2 + k_{y'}^2)$. In Ref. 2, the approximation (23) was used for the $q_{z'}$ integral, thus giving a \tan^{-1} factor in place of the factor in brackets in (26). Making the replacement

$$\frac{2}{\pi} \tan^{-1} \frac{\pi}{f} \rightarrow \frac{2}{f} \left[1 - \frac{1}{f} (1 - e^{-f}) \right],$$

where $f \equiv k_f S$, in Ref. 2 gives the results of the present paper.

Next consider the unpinned modes with $k_z \gg \pi/S$. The same approximation of dropping the cross terms in $G_{x'}$ in (21) can now be used for $G_{z'}$. Thus, the volume Q in (24) is that for which $|q_{z'} - k_{z'}| < \pi/W$, $|q_{y'} - k_{y'}| < \pi/L$, and $|q_{x'} - k_{x'}| < \pi/S$. The integrand $q\theta^2/q^2$ is nearly constant over the volume Q , and its value is $\cong (k_{y'}^2 + k_{x'}^2 \cos^2\theta_m + k_{z'}^2 \sin^2\theta_m)/k^2$. Thus (24) gives

$$\omega_d = 2\pi |\gamma| M_s \left(\frac{k_{y'}^2 + k_{x'}^2 \cos^2\theta_m + k_{z'}^2 \sin^2\theta_m}{k^2} \right). \quad (27)$$

The factor in the parenthesis in (27) is equal to $\sin^2\theta_k$ for

parallel and perpendicular resonance, but not for resonance at an arbitrary angle θ_m . Here θ_k is the angle between \mathbf{k} and \hat{z} . The values of ω_d in (26) and (27) for the special cases of parallel and perpendicular resonance and the corresponding results for circular films are listed in Sec. 10.

For pinned *odd* modes, the analysis leading to (27) is unchanged, and (27) is valid for these modes. For the pinned *even* modes, the integrand in (22) is large in two regions, one near $q_z = k_z$ and the other near $q_z = 0$. The former gives a contribution to ω_d equal to (27). For the latter, consider the value of $G_{z'}$ in (19) in

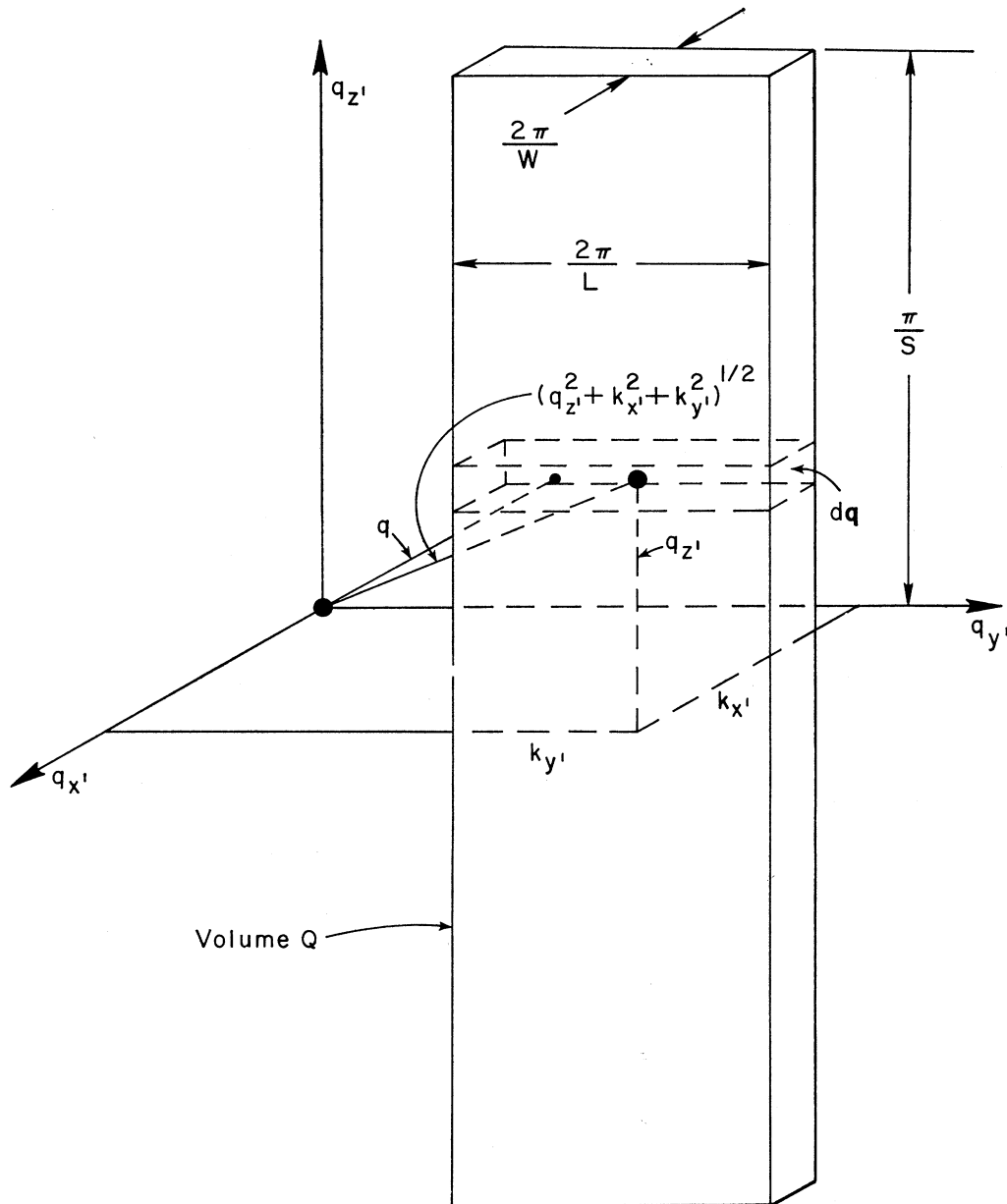


FIG. 2. Volume Q in q space in which the ω_d integrand in (24) is large. The average value $(q_x'^2 + k_x'^2 + k_y'^2)^{1/2}$ of q in the differential volume element dq is shown in the figure.

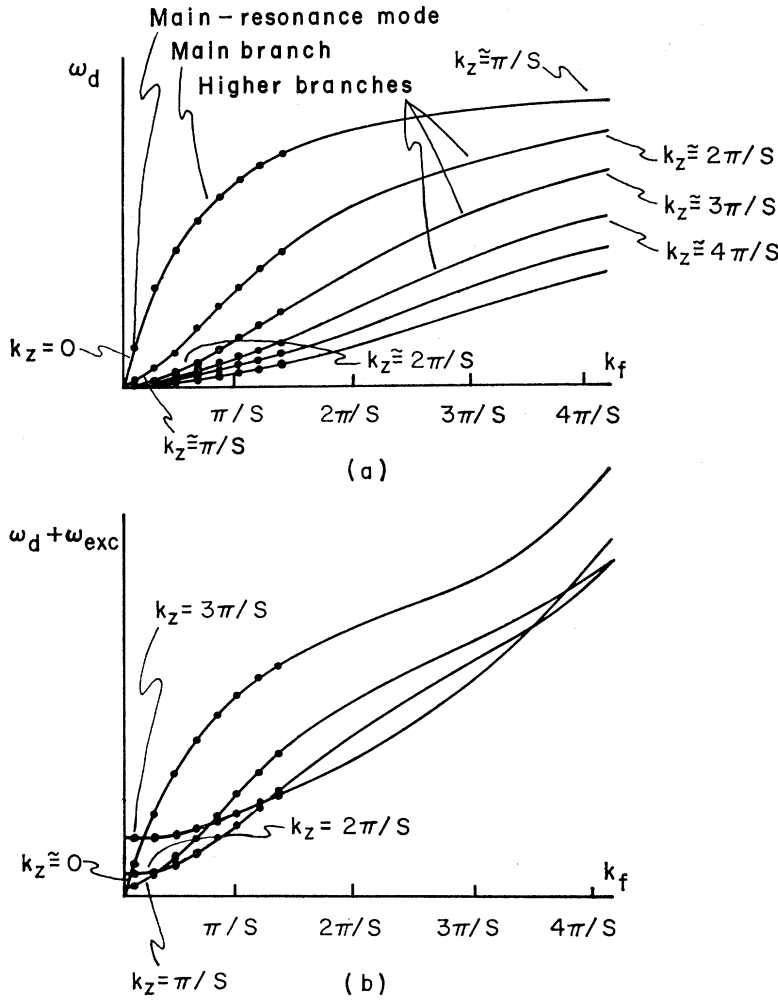


FIG. 3. Sketch of the dispersion relations for the unpinned ferromagnetic modes in a thin film in perpendicular resonance showing the various branches for an infinite film (solid lines) and the individual modes for a finite film (points): (a) for no exchange; (b) schematic effect of exchange.

perpendicular resonance with $k_f S \ll \pi$. From (19), $G_z = 8/k_z^2 S^2$ for $q_z = 0$; thus (22) gives

$$\omega_d \approx \frac{8|\gamma|M_s}{k_z^2 S} \int_{-\infty}^{\infty} dq_z \frac{k_f^2}{q_z^2 + k_f^2}. \quad (28)$$

Evaluating the integral and using $k_z = n_s \pi/S$ gives

$$\omega_d = \frac{8}{\pi} |\gamma| M_s \frac{k_f S}{n_s^2} \quad (29a)$$

for the contribution for the even pinned modes from the region near $q_z = 0$ when $k_f S \ll \pi$ in perpendicular resonance. The joining of this result (29a) onto the results for $k_f S \gg \pi$ will be illustrated in Sec. 5 (Fig. 4).

In perpendicular resonance for the pinned main-branch modes, the result for arbitrary $k_f S$ is

$$\omega_d \approx \frac{8}{\pi^2} \pi |\gamma| M_s k_f S \left(\frac{2}{\pi} \tan^{-1} \frac{\pi}{(8/\pi^2) k_f S} \right) \quad (29b)$$

for pinning, i.e., for $m \sim \cos(\pi z/S)$. In evaluating the

q_z integral leading to (29b) the approximation

$$\frac{1}{2} \left(\frac{\sin \frac{1}{2}(q_z + \pi/S)}{\frac{1}{2} q_z + \pi/S} + \frac{\sin \frac{1}{2}(q_z - \pi/S)}{\frac{1}{2}(q_z - \pi/S)} \right)^2 \approx \frac{\pi^2}{8} \text{ for } |q_z| < \frac{\pi}{(\pi^2/8)S} \approx 0 \text{ otherwise}$$

was made. Thus (29b) is to be compared with

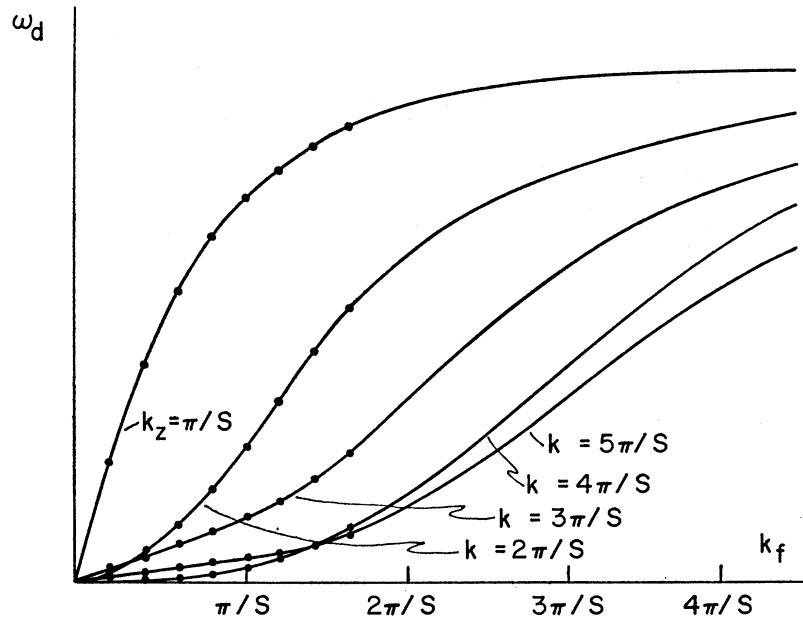
$$\omega_d \approx \pi |\gamma| M_s k_f S \left(\frac{2}{\pi} \tan^{-1} \frac{\pi}{k_f S} \right)$$

for the unpinned case. For $k_f S \ll \pi$, (29b) is $8/\pi^2 = 0.8106$ times smaller than the result for the unpinned main-branch modes.

Consider the errors in (26) resulting from the following approximations used in evaluating the integrals: the neglect of the cross terms in (21), the approximation (23) used in the q_x and q_y integrals, and the replace-

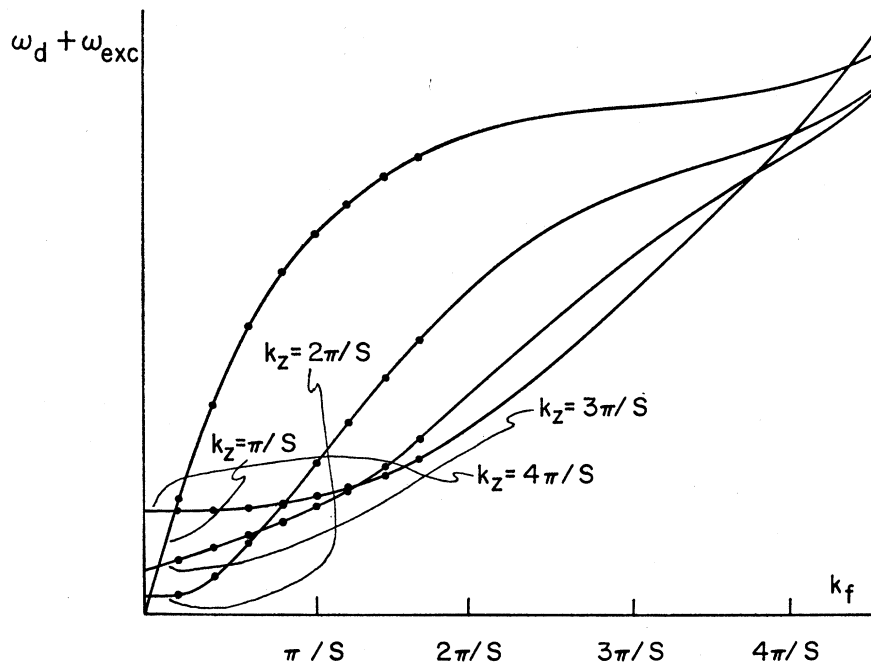
ment of $q_x'^2$ and $q_y'^2$ in (24) by their values $k_x'^2$ and $k_y'^2$ at the center of $d\mathbf{q}$. For large values of n_W and n_L [defined above Eq. (16)], say, $\gtrsim 3$, the approximations are all satisfied fairly well, and the expected errors in ω_d are $\lesssim 10\%$. The greatest error, for $n_L = n_W = 1$, may be considerably greater than 10% because of the replacement of $q_x'^2$ and $q_y'^2$ by $k_x'^2$ and $k_y'^2$. The integrals for the first few modes could be evaluated numerically for

the particular film being investigated if greater accuracy were required. If such evaluations are made, the change in k_x' as a function of $k_f S$ (Sec. 5) should be taken into account in the $I_{z'}$ and $d\mathbf{q}$ integrals in (18). Also, the mode dependence of $\langle H_i \rangle$ (Sec. 6) may account for part of the large spacings of the low-order modes, including that between the main resonance and the weakly excited highest-field mode.² Other



(a)

FIG. 4. Sketch of the dispersion relations for the pinned ferromagnetic modes in a thin film in perpendicular resonance showing the nonzero slopes of the odd modes: (a) for no exchange; (b) schematic effect of exchange.



(b)

factors affecting the over-all accuracy of the results are the deviation of m^+ from the assumed form (15), the approximation used in accounting for the noncircular precession of the magnetization (in Sec. 6), the inhomogeneity in H_i across the thickness of the sample (see Paper IV of the present series), the change in k_x as a function of $k_f S$ (Sec. 5), anisotropy, strain, local spin pinning, line shifts (associated with linewidths), and possibly mode clamping effects.²³ These higher-order effects have been discussed elsewhere.²⁴

5. DISPERSION RELATIONS FOR FINITE AND INFINITE FILMS

Damon and Eshbach¹¹ obtained the dispersion relation for an infinite film (W and L infinite, but S finite) in parallel resonance with no exchange, and Akhiezer and co-workers¹² obtained the corresponding results for an infinite film in perpendicular resonance. It will now be shown that the infinite-film results are closely related to the present results for finite films in the case of no pinning at the large surfaces of the films (at $z' = \pm \frac{1}{2}S$) and have implications concerning the pinning¹ conditions for the trial function for finite films.

The dispersion relations for the normal modes in an infinite film in both perpendicular and parallel resonance are formally the same as those for ordinary spin waves (infinite medium):

$$\omega/|\gamma| = [H_I(H_I + 2\bar{\omega}_d)]^{1/2}, \quad H_I = H_i + Dk^2, \quad (30)$$

$$\omega/|\gamma| \cong H_I + \bar{\omega}_d, \quad \bar{\omega}_d = 2\pi M_s \sin^2 \theta_k, \quad (31)$$

where θ_k is the angle between \mathbf{k} and \hat{z} , and (31) is the circular-precession²¹ approximation to (30). The effect of exchange has been included formally by adding Dk^2 to H_i , as discussed in Sec. 6. For ordinary spin waves all three components of \mathbf{k} are continuous, and it is convenient to consider ω as a function of $|\mathbf{k}|$ with $\sin^2 \theta_k$ as a parameter which varies continuously from 0 to 1 to give a continuous set of curves.²⁵ For an infinite film of finite thickness S , (30) and (31) are still valid and k_x and k_y are still continuous, but k_z has discrete values (for given values of k_x and k_y).

In *perpendicular resonance* in an infinite film, ω is a function of k_z and of $k_f \equiv (k_x^2 + k_y^2)^{1/2}$. Thus, it is convenient to consider ω as a function of k_f with different curves for the different discrete values of k_z . These discrete values of k_z for the even modes are given by the roots of the equation^{12,24}

$$\tan q = \frac{1}{2} k_f S / q, \quad q \equiv \frac{1}{2} k_z S. \quad (32)$$

The corresponding result for the odd modes is $\tan q = -q / \frac{1}{2} k_f S$. The roots of both these equations can be written as

$$k_z = (n_s - p)\pi / S, \quad (16)$$

where $n_s = 1, 3, 5, \dots$ for the even modes, $n_s = 2, 4, 6, \dots$ for the odd ones, and the values of p range between 0 (pinned) for $k_f \gg k_z$ and 1 (unpinned) for $k_f \ll k_z$.

By using (16), (31) and

$$\sin^2 \theta_k = k_f^2 / (k_f^2 + k_z^2), \quad (33)$$

it is easy to obtain the dispersion curves, which are sketched as solid curves Fig. 3(a). Formally replacing the continuous variable k_f by a discrete set (such as $k_f = 0.76\pi/r_0, 1.76\pi/r_0, 2.75\pi/r_0, \dots, (n_f - 0.25)\pi/r_0, \dots$ which corresponds to pinning at the small edges of a circular film—see Sec. 10) and retaining the infinite-film values of k_z from (16) gives a discrete set of points in place of each curve, as illustrated in Fig. 3(a). The curves such as those in Fig. 3 are useful in visualizing the results such as (26) and (27), as discussed in Sec. 10. Figure 3 (and Figs. 4 and 12) are sketches, not exact plots.

We now show that this formal procedure of replacing curves by an appropriate set of discrete points gives agreement with the results of the variational calculation for two limiting cases of $k_f S$ for unpinned modes (but not for pinned ones). First consider perpendicular resonance and the top curve in Fig. 3(a), which corresponds to $n_s = 1$ in (16). For the case of $k_f S \ll \pi$, we can set $\tan q \cong q$ in (32), which gives $q^2 = \frac{1}{2} k_f S$, or

$$k_z = [(2/\pi^2)k_f S]^2 \pi / S. \quad (34)$$

In passing, note that $k_z \ll \pi/S$; therefore, m^+ is nearly constant (i.e., unpinned) across the thickness of the film for this case of $k_f S \ll \pi$ and $n_s = 1$. This result and the result below that m^+ is nearly pinned for $k_f S \gg \pi$ and $n_s = 1$ are explained physically in Sec. 7. Substituting (34) and (33) into (31) gives

$$\omega/|\gamma| = H_i + \pi M_s k_f S \quad (35)$$

in agreement with (44a) in the limit $k_f S \ll 1$.

In the other limit of $k_f S \gg \pi$ (still with $n_s = 1$), (32) gives $q \cong \pi/2$, or $k_z = \pi/S$; therefore, $k_f^2 \gg k_z^2$. With this result, (31) and (33) give $\omega_d \cong 2\pi|\gamma|M_s$, in agreement with (44a) in the limit $k_f S \gg 1$. The agreement of the two results in the limit $k_f S \gg 1$ is not surprising since both the variational-calculation and modified-infinite-film results are expected to be accurate in this limit. However, it appears that the errors in the modified-infinite-film results should be rather large for the low-order modes [n_L and n_W small—see Eq. (16)], and the errors in the variational expression also are expected to be large for these modes as discussed in Sec. 4. The most accurate results for the low-order modes should be those obtained from numerical evaluations of the integrals in Sec. 4; the variational calculation takes into account the sources of the microwave demagnetization field in the finite sample, while the formal application of the infinite-film results to a finite film implies replacing integrals over one half cycle of a sine wave by integrals from $-\infty$ to ∞ . For the other curves in Fig. 3, results

²³ M. Sparks, Quart. Appl. Math. (to be published).

²⁴ M. Sparks, Solid State Commun. (to be published).

²⁵ For example, see Fig. 3.2 of Sparks (Ref. 20).

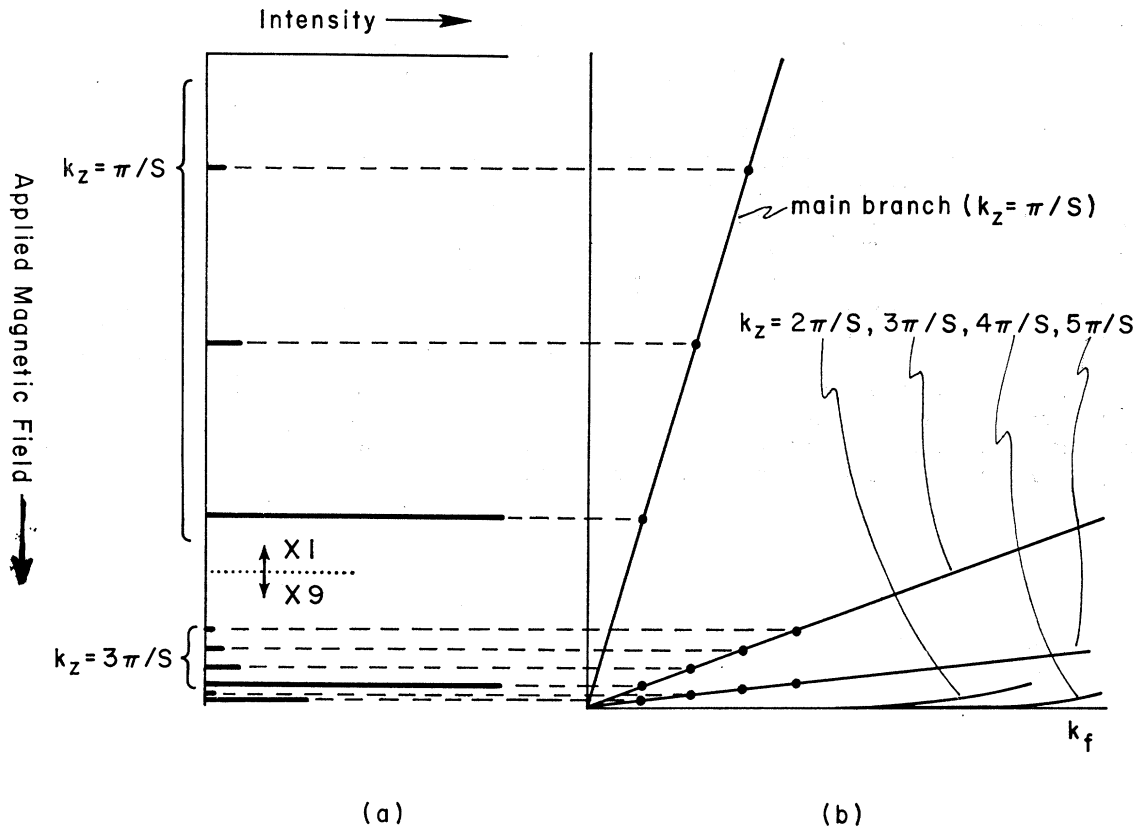


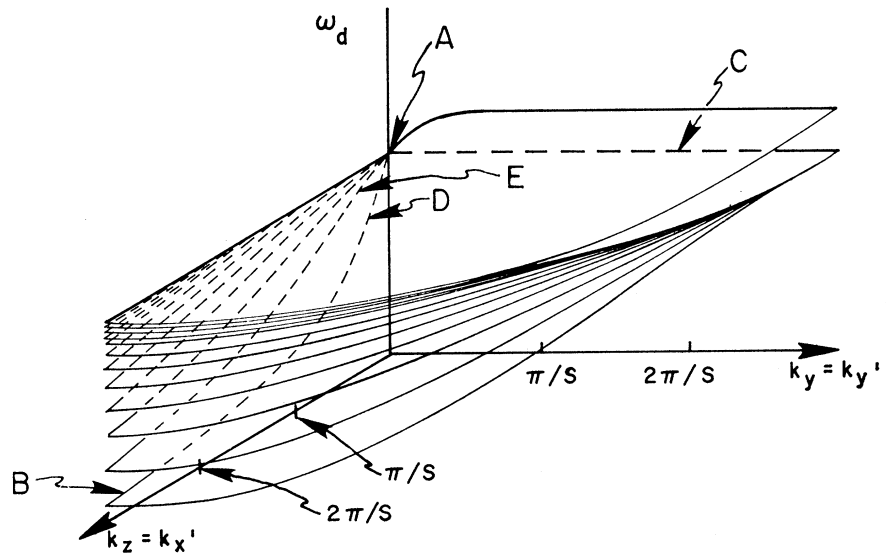
FIG. 5. (b) Enlarged view of the portion of Fig. 4(a) near the origin. (a) Intensities and spacings of several of the modes shown in (b).

(44b) are already in a form which shows its equivalence to (31).

Further disadvantages of the modified-infinite-film results are that these results are incorrect for pinned modes, the effect of changing the amount of pinning at the small edges of the sample cannot be obtained from

the theory, the important effects of an inhomogeneous H_i (discussed in Sec. 6) are not included, the effect of the deviation of m from that of an infinite film is not contained in the theory, and there is no direct way to improve the accuracy of the results. The usual infinite-film results^{11,12} apply only to the unpinned modes in

FIG. 6. Dispersion relations for the magnetostatic modes of an infinite film in parallel resonance reproduced from Fig. 3 of the paper by Damon and Eshbach (Ref. 11). The single sheet which intersects the $\omega_d - k_y$ plane above the line marked A-C is a surface-mode sheet and the others are bulk-mode sheets.



rectangular samples in the limiting cases of $\theta_m=0$ and $\pi/2$. However, Sparks has solved the infinite-film problem in circular-cylindrical coordinates and applied the results formally to finite circular films.²⁴

The series of modes having the smallest value of k_z will be called the main series, or modes of the *main branch* (see Fig. 3). The main-branch mode having the smallest value of k_f will be called the *main-resonance mode*. The other branches (marked $k_z=\pi/S, 2\pi/S, \dots$ on the low-frequency section of Fig. 3) will be called *higher branches*. The value of k_z for a given branch increases by π/S as k_f goes from 0 to ∞ for an infinite film, as marked at the top and bottom of Fig. 3. We mention in passing that in an infinite film in perpendicular resonance with no explicit pinning mechanism the modes with $k_f S \ll n_S \pi$ are unpinned, and those with $k_f S \gg n_S \pi$ are pinned. The same result is expected

to be true in finite films. In particular, the modes with $k_f S \gg n_S \pi$ are expected to be pinned even in the absence of an inhomogeneous M_s , antiferromagnetic surface layer, surface anisotropy, etc. This is of no consequence in experiments performed to date since only modes with $k_f S \ll \pi$ have been observed.

The dispersion relation for pinned modes in perpendicular resonance are similar to those of unpinned modes (Fig. 3) except that the even higher-order branches have nonzero slopes at $k_f=0$ according to (29). Figure 4 illustrates this result. Figure 5(b) is an enlarged view of the low- k_f portion of Fig. 4. The mode intensities in Fig. 5(a) are discussed in Secs. 8–10, and the effect of Portis pinning⁵ is discussed in Sec. 7.

The dispersion relation for parallel resonance cannot be displayed as a single set of curves (as in Fig. 3 for perpendicular resonance) because the frequency is a

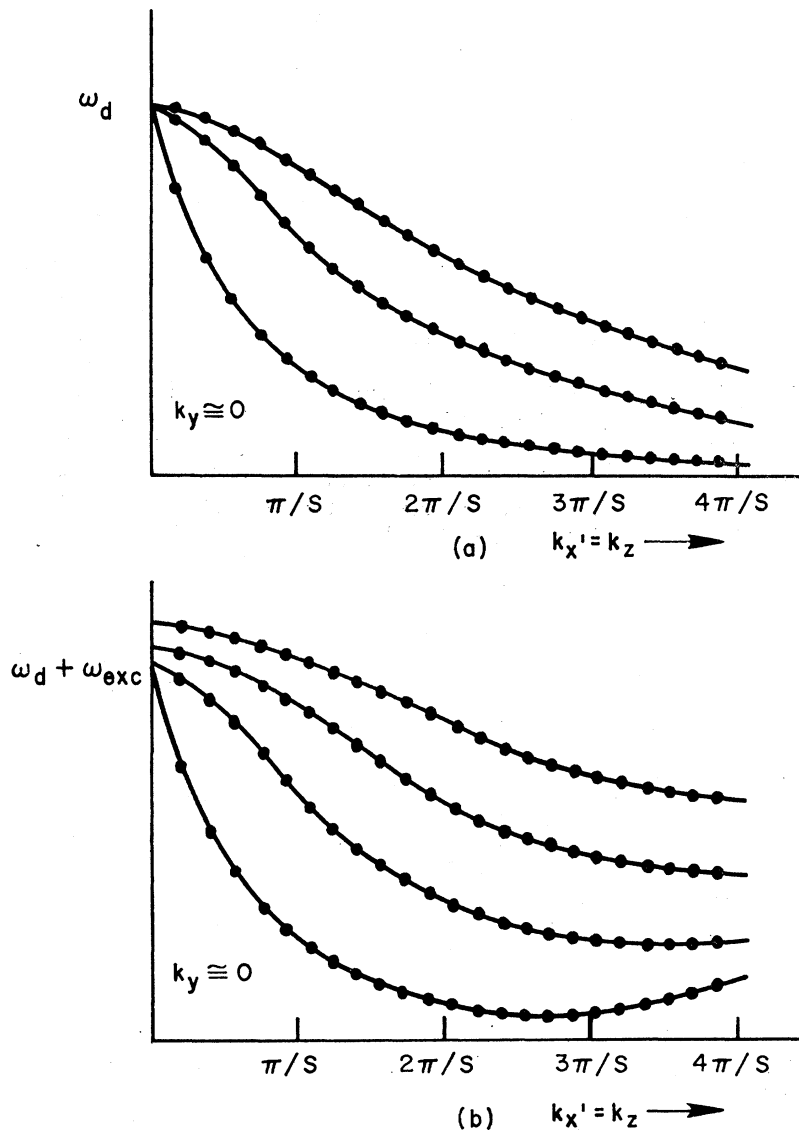


FIG. 7. $k_y=0$ plane of Fig. 6. The solid curves (for an infinite film) in (a) are reproduced from Fig. 4 of the paper by Damon and Eshbach (Ref. 11). The points are for a finite film: (a) for no exchange; (b) schematic effect of exchange.

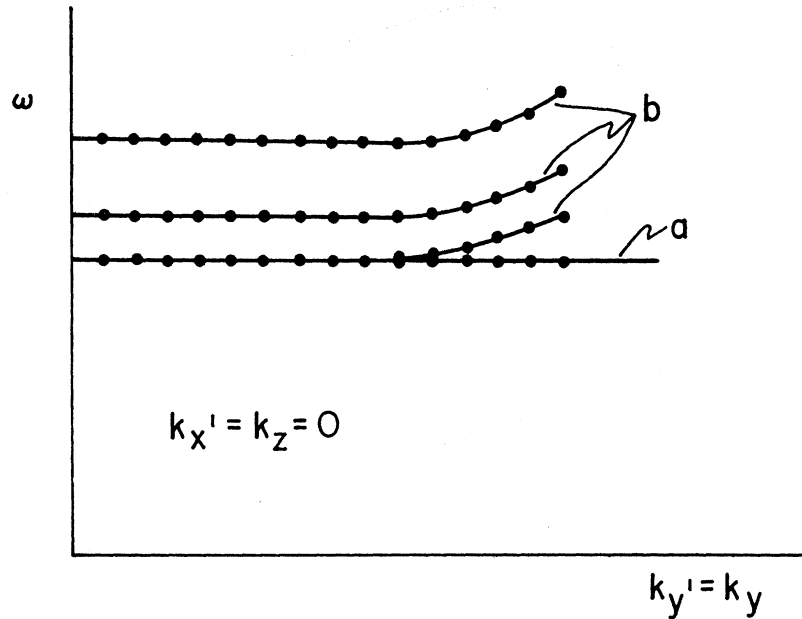


FIG. 8. $k_z=0$ plane of Fig. 6 showing the infinite-film results as solid curves and the finite-film results as points. Curve (a) is for no exchange (all modes degenerate) and (b) schematically illustrates the effect of exchange.

function of $\cos^2\phi' \equiv k_x'^2/(k_x'^2+k_y'^2)$ as well as k_f and k_z' . It can be represented by sets of curves in (ω, k_x', k_z') space, as shown in Fig. 6, which is reproduced from the paper of Damon and Eshbach.¹¹ The intercepts of these surfaces with a plane of constant k_y' , gives ω as a function of k_x' for this value of k_y' , as illustrated in Fig. 7 for the smallest value of $k_y' = \pi/L$. The intersections of the surfaces with the plane of constant k_z' , gives ω as a function of k_y' for this value of k_z' , as illustrated in Fig. 8(a) for $k_z' = 0$.

In view of the fair agreement between the theoretical results of Secs. 4 and 5 with the infinite-film results, it appears likely that the frequencies of the surface modes in finite films can be approximated by replacing the continuous variables k_x' and k_y' by the same discrete set used for the bulk modes. This gives the results illustrated schematically in Fig. 9(a) for the surface modes for the case of $k_f = k_y$. The experimental results of Brundle and Freedman¹⁶ have been analyzed²⁴ using this method, and it has been suggested that several low-field modes in Fig. 3 of Ref. 2 are surface modes.²⁴

In both parallel and perpendicular resonance, the magnetostatic modes having $k_f \ll k_z'$ are nearly unpinned, and those having $k_f \gg k_z'$ are nearly pinned.^{11,12} In parallel resonance the magnetostatic modes having $k_f \ll k_z'$ also show a change in symmetry (even or odd functions of x , where $x=0$ at the center of the film) as the angle $\phi \equiv \tan^{-1}(k_y/k_z)$ changes. Here the applied field is along z , and the x axis is normal to the plane of the film. From the results of Damon and Eshbach¹¹ [their Fig. 7 and Eqs. (20), (11), (16), and (17)] it can be shown that for $0 < k_y \ll \pi/S$, m for the main-branch changes from $m \approx \sin(\pi x/S)$ (unpinned, odd) for $k_z \gtrsim k_y \sqrt{\Omega_H}$, to $m \approx 1$ (unpinned, even) for $k_y/\sqrt{\Omega_H} \lesssim k_z \ll \pi/S$, to $m \approx \cos(\pi x/S)$ (pinned, even) for $k_z \gg \pi/S$.

Here $\Omega_H \equiv H_i/4\pi M_s$. For the main branch in the limit of $k_z \rightarrow 0$, $m \approx \sin(\pi x/S)$ for $k_y \ll \pi/S$, and $m \sim \cos(\pi x/S)$ for $k_y \gg \pi/S$. These results are illustrated schematically in Fig. 10.

The higher branches show corresponding symmetry changes at $k_z \cong k_y/\sqrt{\Omega_H}$ for small values of k_y . Note that $k_z < k_y/\sqrt{\Omega_H}$ is the region in which the surface states exist, and $k_z \gtrsim k_y/\sqrt{\Omega_H}$ is the region in which bulk modes are excited when k_f is small and the applied microwave field is independent of x . For $k_f S \lesssim 1$, the surface modes extend across the sample, i.e., they do not cling tightly to the surface, and they have large intensities. Thus for $k_f S \ll \pi$, the magnetostatic modes

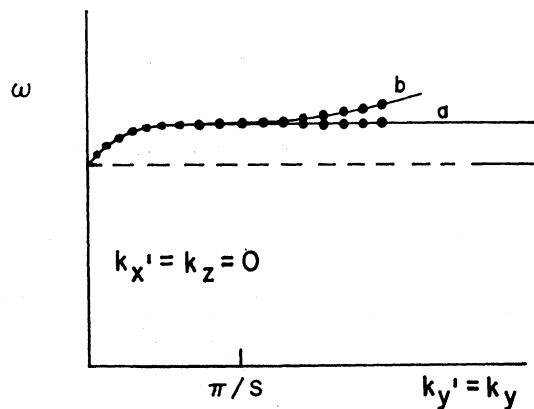


FIG. 9. Magnetostatic surface modes with $k_z=0$ in an infinite film in parallel resonance. The solid curve (a) (for an infinite film with no exchange) is reproduced from Fig. 3 of the paper by Damon and Eshbach (Ref. 11). It is speculated that the points should represent the magnetostatic surface-mode frequencies in a finite film. Curve (b) schematically illustrates the effect of exchange.

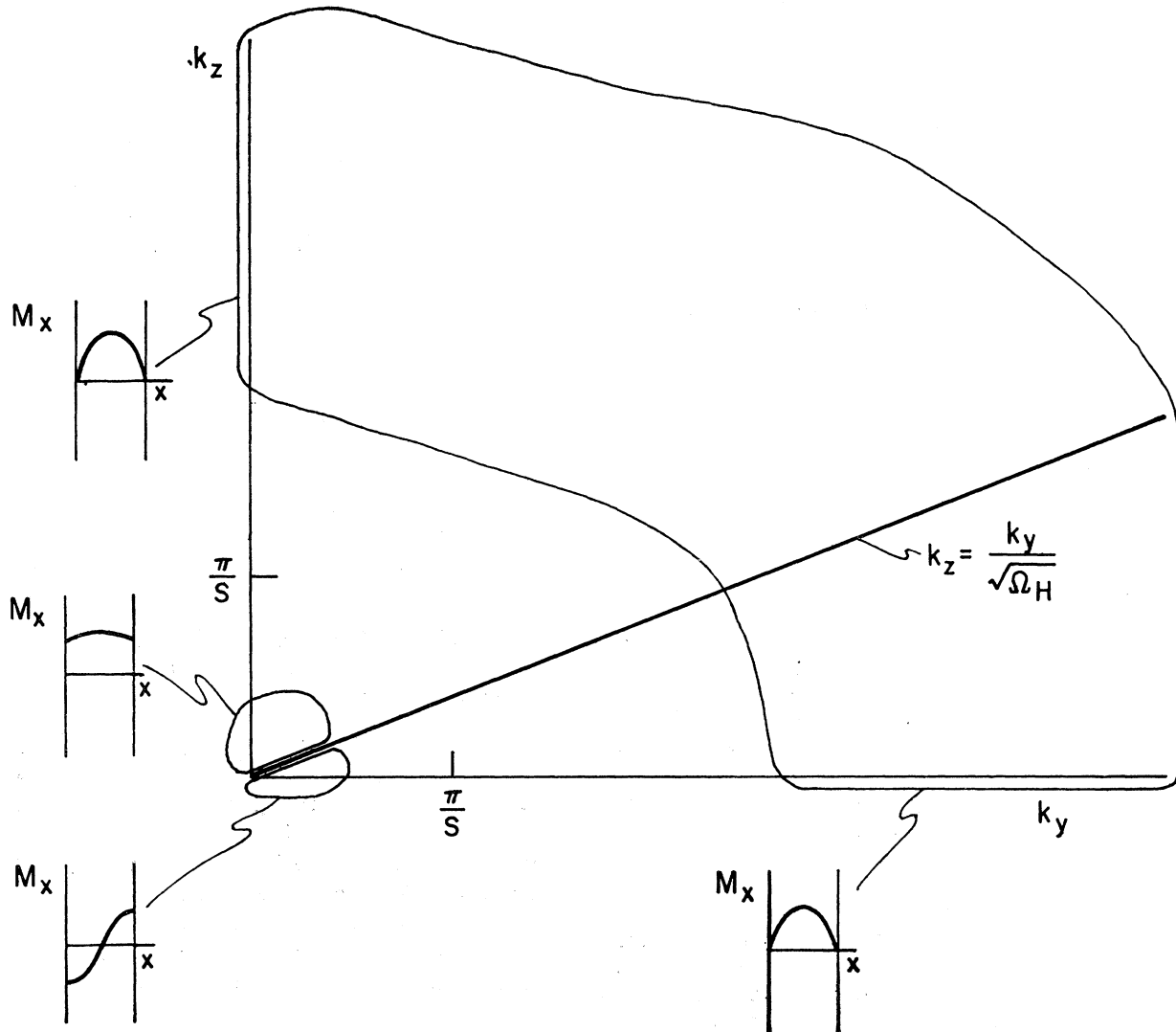


FIG. 10. Schematic illustration of the change from unpinned to pinned surface conditions as k_f increases through $k_f = \pi/S$ and of the change of symmetry of the magnetization at $k_z/k_y \cong \sqrt{\Omega_H}$ for $k_f S \ll \pi$. Here $\Omega_H = H_i/4\pi M_s$.

which are strongly excited by a constant applied microwave field are surface modes when $k_z \lesssim k_y/\sqrt{\Omega_H}$ and are main-branch bulk modes when $k_z \gtrsim k_y/\sqrt{\Omega_H}$.

For $k_f S \gg \pi$, the surface modes cling tightly to the surface,¹¹ while the main-branch bulk modes have $\mathbf{m} \sim \cos(\pi x/S)$. Thus the bulk modes have the largest intensities for all values of k_z/k_y when $k_f S \gg \pi$. The contradictory conclusions of Wolfram and De Wames¹⁴ were based on computer calculations for specific cases which were incorrectly generalized.

6. EFFECTS OF EXCHANGE, NONCIRCULAR PRECESSION OF MAGNETIZATION, AND INHOMOGENEOUS H_i

First consider the effect of exchange on the normal-mode frequencies in an infinite film (W and L infinite,

but thickness S finite) in perpendicular resonance. The solutions to (6) with no exchange ($\Lambda = 0$) are products of sine waves for rectangular coordinates and are circular-cylindrical functions [Eq. (49)] for circular-cylindrical coordinates. Since $-\nabla^2 m^\pm = k^2 m^\pm$ in both cases ($k^2 = k_\rho^2 + k_z^2$ for circular films²⁶), $-\nabla^2$ can be replaced by k^2 in (6), and the solutions for $\Lambda = 0$ are also solutions for $\Lambda \neq 0$. Consequently, it might appear that an *exact* solution could be obtained for an infinite film by formerly replacing \bar{H}_i by $\bar{H}_i + \Lambda k^2$ in the solution for the case $\Lambda = 0$; symbolically

$$\bar{H}_i \rightarrow \bar{H}_i + \Lambda k^2. \quad (36)$$

²⁶ Since $k^2 = k_\rho^2 + k_z^2$, it might appear that the exchange energy is independent of the number l of azimuthal nodes. However, the values of k_ρ are determined by the zeroes of $J_l(k_\rho r_0)$, and these zeroes depend on the value of l .

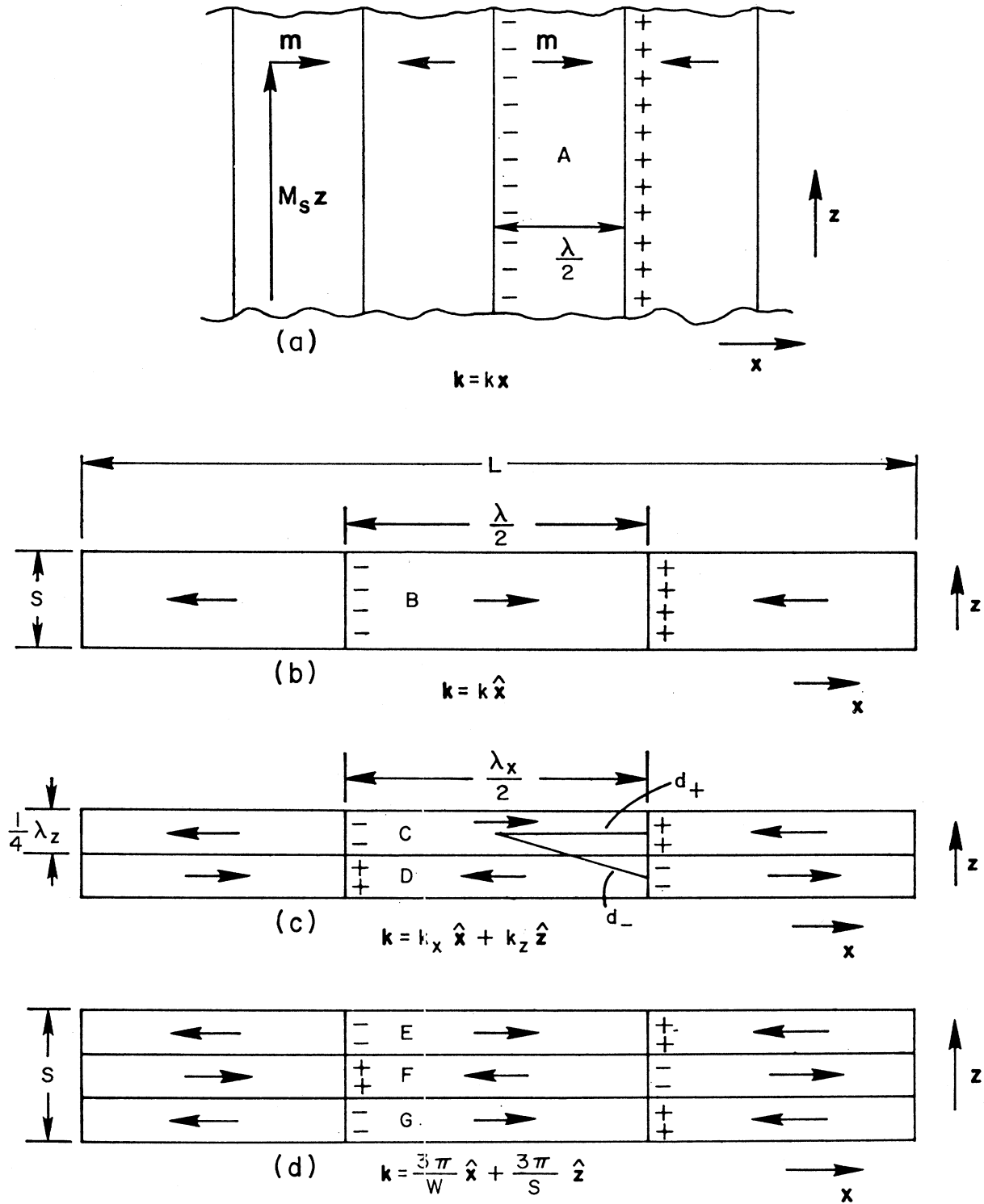


FIG. 11. Schematic illustration of the microwave magnetization m showing only the values of m which are one-half wavelength apart: (a) for an ordinary spin wave (infinite medium); (b) for a finite film with $k_z=0$ and $\lambda_x/2 \gg S$; (c) for a finite film with $k_z=\pi/S$ and $\lambda_x/2 \gg S$; (d) for a finite film with $k_z=3\pi/2S$ and $\lambda_x/2 \gg S$. The plus and minus signs signify magnetic sources of demagnetization field h for equivalent slab samples as discussed in the text.

However, this formal procedure neglects the effect of exchange on the pinning conditions at $z' = \pm \frac{1}{2}S$, as discussed in Sec. 9.

In some simple cases, which fortunately include most cases of present interest to experimentalists, the effects of exchange are intuitively clear. For example, for an infinite film in perpendicular resonance with $\Lambda=0$, $dm^+/dz \cong 0$ at $z = \pm \frac{1}{2}S$ when $k_f S \ll \pi$ for the main branch or when $k_f \ll k_z$ for the higher branches. A simple argument¹⁷ indicates that exchange also tends to make the slope small at the boundary for long-wavelength modes ($k_z a \ll 1$, where a is the lattice spacing). Thus exchange does not tend to change the boundary conditions at $z = \pm \frac{1}{2}S$, and it is reasonable to expect that the formal replacement (36) will give accurate results for the normal-mode frequencies. In this particular case, the magnetization m^+ also will be relatively unchanged from that for $\Lambda=0$. For the other extreme of $k_f S \gg \pi$ for the main-resonance mode, or $k_f \gg k_z$ for the higher-branch modes, $m^+ \cong 0$ at $z = \pm \frac{1}{2}S$, rather than $dm^+/dz = 0$, when $\Lambda=0$. In this case the exchange does change the boundary conditions at $z = \pm \frac{1}{2}S$, and m^+ will be changed from its form for $\Lambda=0$. (See Sec. 9).

For an infinite film, this change in m^+ can be substantial, but the frequencies are relatively unchanged from those in (30) (away from the crossovers).^{24,14} This is not surprising since the physical arguments of Sec. 7 indicate that the demagnetization contribution to ω still should be $\sim 2\pi\gamma M_s$, and the exchange contributions should be of the order of Dk^2 since the modes still can be characterized by the number of nodes in m^+ and first-order changes in m^+ tend to give second-order changes in ω in general. From (36) it is seen that the central effect of exchange on the dispersion curves is obtained simply by adding $Dk^2 = D(k_{z'}^2 + k_f^2)$ to all curves. The term $Dk_{z'}^2$ increases the value of the $k_f=0$ intercepts, and the term Dk_f^2 adds a quadratic factor to the curves, as illustrated in the (b) parts of Figs. 3, 4, and 7-9.

In passing, it should be mentioned that $k_{z'}$ is imaginary for a surface wave. That is,

$$m^+ \sim \exp[i(k_{z'}|z')z'] \sim \exp[-|k_{z'}|z].$$

Thus, the exchange term Dk^2 becomes $D(k_f^2 - |k_{z'}|^2)$. For pure exchange surface waves (demagnetization energy neglected), this result is correct.²⁷ However, formally adding $D(k_f^2 - |k_{z'}|^2)$ to the energy of the magnetostatic surface waves¹¹ gives an incorrect result. For example, $k_f^2 = |k_{z'}|^2$ for a DE surface wave propagating in the direction perpendicular to the applied field; thus $D(k_f^2 - |k_{z'}|^2) = 0$, and this wave would have no exchange-energy contribution to its frequency, which is incorrect. The form of m^+ for magnetostatic waves is changed considerably when exchange is added, as discussed in Sec. 9, and the result is that the dispersion

curve does bend up with increasing k_f as illustrated schematically in Fig. 9(b).

Next consider the effect of the noncircular precession of the spins. For infinite-medium spin waves, the dispersion relation is given by (30), and the circular-precession approximation²¹ to (30) is (31). The error introduced by making this approximation is zero at the bottom of the manifold (i.e., at $\theta_k=0$) and is maximum at the top of the manifold ($\theta_k=\pi/2$). See Fig. 3.2 of Ref. 20. The error at $\theta_k=\pi/2$ decreases as H_I increases, i.e., as either H_i or Dk^2 increases. For YIG at 9.40 GHz and room temperature in perpendicular resonance with $Dk^2=0$, the error in the applied field at the top of the band is 2.6% (2593+1750 Oe without the approximation and 2481+1750 Oe with the approximation) and the error in the width of the manifold is 14.7% (763 Oe without the approximation and 875 Oe with the approximation).

In order to account for the noncircular precession approximately in the present case of a finite sample, the circular precession result (10) can be formally replaced by (30) with $H_I = \langle H_i \rangle + \bar{\omega}_{\text{exc}}$. In the limit as L and W approach infinity and $H_i = \text{const}$, this procedure gives accurate results. Although (30) is not exact for finite films, it is expected to be within the over-all accuracy of ~ 5 - 10% of the theory for YIG at X band or higher frequencies. Without any correction for noncircular precession, the errors are fairly small, as discussed above, and the corrected result (30) gives accurate results in several limiting cases (e.g., $\bar{\omega}_d \ll 875$ Oe, or n_L and $n_W \gg 1$).

In general there will be inhomogeneities in H_i across the thickness^{3,5,17} S and along the radius r_0 (or length and width) of the film. These inhomogeneities change the values of $\langle H_i \rangle$ and of $\bar{\omega}_d = \omega_d/|\gamma|$. The inhomogeneity across S can give rise to Wigen-Kooi-type pinning³ (near the surfaces) or to Portis-type pinning⁵ (in from the surfaces). The Portis-type pinning changes the exchange and internal field terms in ω , as is well known.⁵ It also changes ω_d since the effective thickness S_{eff} over which \mathbf{m} is large is less than S (see Fig. 12 below), and it makes the slope of ω versus k_f nonzero at $k_f=0$ for even modes, as discussed in Sec. 7. The inhomogeneity in H_i across S , as well as sources of the inhomogeneity, will be considered further in Paper IV.

It is difficult to calculate accurately the effects on ω of the inhomogeneity since it is difficult to calculate both the spatial dependence of $\mathbf{H}_i(\mathbf{r})$ and the effect of the inhomogeneity on \mathbf{m} . However, the qualitative features can be determined as follows: To be concrete, consider the variation in \mathbf{H}_i along r_0 for the magnetostatic modes in perpendicular resonance in a circular film with $S/2r_0 \lesssim \frac{1}{10}$. The value of demagnetization field $H_D = 4\pi M_s - \delta H_D$, where $H_i = H_{\text{app}} - H_D$, near the center of the film is fairly constant. For example, the value of H_D inside the thin disk along its axis is

$$H_D(0) \cong 4\pi M_s [1 - (S/2r_0)] \quad (36')$$

²⁷ M. Sparks, J. Appl. Phys. **41** (1970); Phys. Rev. (to be published).

for sufficiently large values of H_{app} to hold \mathbf{M}_s approximately along \hat{z} .

At the edge of the disk in the center plane [i.e., at $\rho \equiv (x^2 + y^2)^{1/2} = r_0$ and $z = 0$], $H_D \cong 2\pi M_s$, and at $\rho = r_0$ and $z = \pm \frac{1}{2}S$, $H_D \cong 3\pi M_s$. Most of the reduction in the size of H_D from its center value (36') to its edge value occurs within the range $r_0 - 2S \lesssim \rho < r_0$. In order to obtain a guide in estimating the sizes of $\langle \delta H_D \rangle$ and $\bar{\omega}_d$, the variation in H_D will be approximated by

$$H_D(\rho) - H_D(0) \cong \frac{3}{2}\pi M_s \exp[-(r_0 - \rho)/S] \quad (36'')$$

The value $\frac{3}{2}\pi M_s$ at $\rho = r_0$ was chosen as the average of the values given above for $z = 0$ and $z = \frac{1}{2}S$. The value of H_D from (36'') (with $\frac{3}{2}\pi M_s$ replaced by $2\pi M_s$ to account for $z = 0$) fits the numerical results of Fig. 13 of Ref. 28 for $z = 0$ and $S/r_0 = 0.2$ to within $\sim 10\%$ or better for all ρ .

Just as the Portis-type pinning changes S_{eff} for the low-order modes, it is reasonable to expect that the inhomogeneity in \mathbf{H}_i along r_0 will change the effective radius r_{eff} over which \mathbf{m} is large for the low-order modes. The reason for the reduced effective radius is that the spins near $\rho = r_0$ see different values of H_i and h from those in main bulk of the film; thus the amplitude of \mathbf{m} near $\rho = r_0$ is expected to be small since these edge spins are off resonance, roughly speaking.

The microwave demagnetization factor $\bar{\omega}_d$ can be written as

$$\bar{\omega}_d = \bar{\omega}_d(r_0) + \delta\bar{\omega}_d,$$

where $\bar{\omega}_d(r_0)$ is the value of $\bar{\omega}_d$ when $r_{\text{eff}} = r_0$ formally, and $\delta\bar{\omega}_d$ is the shift resulting from the reduced effective radius. The size of $\delta\bar{\omega}_d$ can be estimated roughly by replacing r_0 in (27), (44), etc., by r_{eff} and formally estimating the size of r_{eff} as the value of ρ at the turning point at which

$$H_D(r_{\text{eff}}) - H_D(0) = \bar{\omega}_d + Dk^2 \quad (36''')$$

The values of the left- and right-hand sides of (36''') are calculated for $r_{\text{eff}} = r_0 - 2S$, using the approximation (36''). If $H_D(r_{\text{eff}}) - H_D(0) < \bar{\omega}_d + Dk^2$, a larger value of r_{eff} is chosen, and the process is repeated until self-consistency is obtained. For example, for $2r_0/S = 15$, $r_{\text{eff}} = r_0 - 2S$, and Dk^2 negligible, (36'') gives $H_D(r_{\text{eff}}) - H_D(0) = 118$ Oe and (53) gives $\bar{\omega}_d = 114$ Oe for the main-resonance mode. For $r_{\text{eff}} = r_0 - 2.03S$, both $H_D(r_{\text{eff}}) - H_D(0)$ and $\bar{\omega}_d \cong 115$ Oe, as the self-consistent value of $\bar{\omega}_d$. The value of $\bar{\omega}_d(r_0)$ is 86 Oe, giving $\delta\bar{\omega}_d \cong 29$ Oe, as a rough estimate. For the high-order modes (large k_f), $\bar{\omega}_d \cong 2\pi M_s$, and $r_{\text{eff}} \cong r_0$; therefore, $\delta\bar{\omega}_d \cong 0$. For the low-order, higher-branch modes $\bar{\omega}_d \ll 2\pi M_s$, and $\delta\bar{\omega}_d \cong 0$.

In order to obtain a simpler, but somewhat less accurate, approximation to $\delta\bar{\omega}_d$ for the uniform precession in perpendicular resonance, $\bar{\omega}_d$ in (53) or (44a) is expanded

in the small- $k_f S$ limit, giving $\bar{\omega}_d \sim k_f S \sim S/r_{\text{eff}}$. With $r_{\text{eff}} \cong r_0 - 2S$ and $1/(r_0 - 2S) \cong (1/r_0)[1 + (2S/r_0)]$, this gives $\bar{\omega}_d \cong \bar{\omega}_d(r_0)[1 + (2S/r_0)]$; i.e.,

$$\delta\bar{\omega}_d \cong (2S/r_0)\bar{\omega}_d(r_0), \quad (36''''')$$

for the main-resonance mode. For the example above with $2S/r_0 = 4/15$ and $\bar{\omega}_d(r_0) = 86$ Oe, (36''''') gives $\delta\bar{\omega}_d \cong 23$ Oe, which is within the expected accuracy of the previous value of 29 Oe.

A very rough guide in determining the values of $\langle \delta H_D \rangle$ can be obtained as follows: For the main-resonance mode, the weighting factor $|m_n^+|^2$ in $\langle H_i \rangle$ is large near the center of the disk, where $H_D \cong H_D(0)$, and is small near the edges. Thus $\langle H_D \rangle$ is slightly less than $H_D(0)$, and (36') and (36'') give $\langle \delta H_D \rangle = g_{mr} \times (S/2r_0)(4\pi M_s)$, where g_{mr} is slightly greater than 1. For example, a rough numerical evaluation of the integral $\langle H_i \rangle$ using the curves in Figs 12 and 13 of Ref. 28 for $(S/2r_0) = 0.1$ (the smallest value given) gives $g_{mr} \cong 1.1$. The weighting factor was taken as $[J_0(0.76\pi/r_{\text{eff}})]^2$, where $r_{\text{eff}} = 0.75r_0$. The high-order modes have many oscillations along r_0 , and $[\rho|m_n^+|^2]^{1/2}$ is sinusoidal over most of the sample. Therefore the weighted average,

$$\langle H_i \rangle \sim \int_0^{r_0} d\rho \rho |m_n^+|^2 H_i,$$

is approximately equal to the unweighted average,

$$\sim \int_0^{r_0} d\rho H_i.$$

With (36'') this gives

$$\langle \delta H_D \rangle = g(S/2r_0)(4\pi M_s), \quad (36''''''')$$

with $g = g_{ho} \cong 7/4$ for the high-order modes. This result (36'''''''), with $g = g_{mr}$, is valid for the main-resonance mode. For the low-order higher-branch magnetostatic modes, the value of g in (36''''''') is approximately 1 since $\bar{\omega}_d + Dk^2 \cong 0$, making r_{eff} smaller than that of the main resonance so that H_D is closer to $H_D(0)$.

For a YIG disk ($4\pi M_s = 1750$ Oe) with $S/2r_0 = \frac{1}{15}$, (36''''''') gives $\langle \delta H_D \rangle \cong 130$ Oe for the main-resonance mode and 205 Oe for the higher-order modes. The value of g_{mr} was taken as 1.1. In general, $\langle \delta H_D \rangle$ and $\bar{\omega}_d$ for the main-resonance mode both are approximately proportional to $(S/2r_0)(4\pi M_s)$, and they have approximately the same values. In the present example with $S/2r_0 = \frac{1}{15}$, the values are $\bar{\omega}_d \cong 115$ Oe and $\langle \delta H_D \rangle \cong 130$ Oe. Notice that $\langle \delta H_D \rangle$, $\bar{\omega}_d$, and $\delta\bar{\omega}_d$ all reduce the value of the field for resonance H_{app} .

Consider the general effects of $\langle \delta H_D \rangle$ and $\delta\bar{\omega}_d$ on the spacings of the magnetostatic modes in perpendicular resonance. Since the values of g in (36''''''') range between ~ 1 and $\sim 7/4$, it is convenient to write

$$\langle \delta H_D \rangle = (S/2r_0)(4\pi M_s) + (g-1)(S/2r_0)(4\pi M_s). \quad (37)$$

²⁸ R. I. Joseph and E. Schlömann, J. Appl. Phys. 36, 1579 (1965).

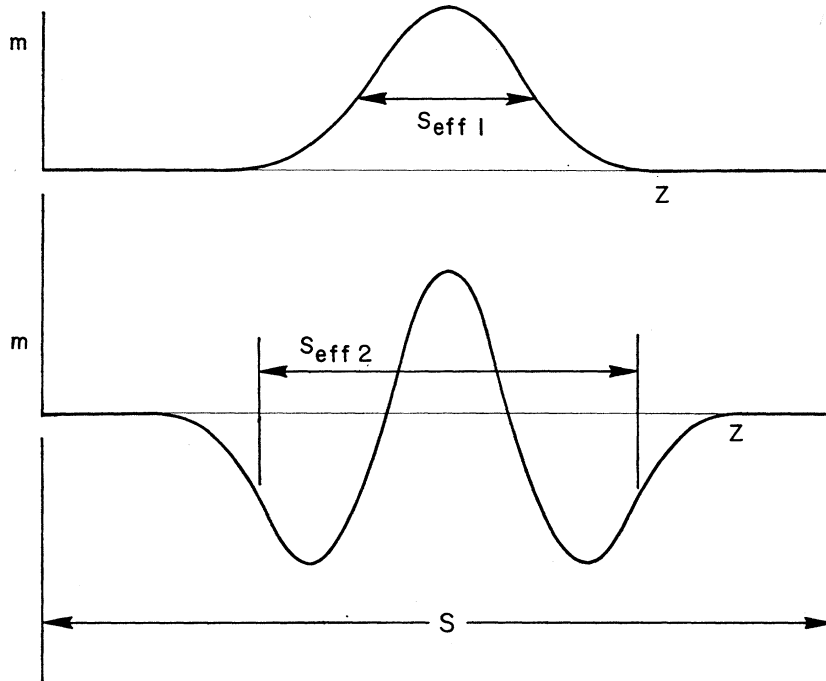


FIG. 12. Schematic illustration of the magnitude of the microwave magnetization m for the first and third modes of Portis (Ref. 5) illustrating that the effective thickness S_{eff} of the film, which determines the magnetostatic mode spacing, is less than the physical thickness S for the Portis-pinned modes.

The first term shifts the fields for resonance of all modes down by $(S/2r_0)(4\pi M_s)$ in the circular-precession approximation. The second term in (37) has little effect on the highest-field modes (the low-order higher-branch modes), while it shifts the high-order modes [having $\bar{\omega}_d(r_0) \cong 2\pi M_s$] to lower field, thus increasing the width of the normal-mode manifold by $\sim \frac{3}{4}(S/2r_0)(4\pi M_s)$ and increasing the spacings between the low-order main-branch modes and between the main-resonance mode and the highest-field modes.

The term $\delta\bar{\omega}_d$ also is approximately equal to zero for the highest-field modes and increases the spacing between the main-resonance mode and the highest-field mode. But it does not change the width of the manifold, and it reduces the spacings between the low-order main-branch modes, thus partially cancelling the (larger) increase caused by $\langle\delta H_D\rangle$. For the example above with $S/2r_0 = \frac{1}{15}$ and $4\pi M_s = 1750$ Oe, the value of the largest increase in spacing (between the main-resonance mode and the highest-field mode) is $(0.1)\frac{1}{15}(1750) + 29 \cong 40$ Oe, as a rough estimate.

7. INTUITIVE EXPLANATION OF RESULTS

All of the results of Secs. 4 and 5 can be understood intuitively by considering a simple model of a square film of dimensions $L \times L \times S$ in perpendicular resonance. In order to understand the behavior of ω_d , first recall that for an ordinary spin wave with wave vector \mathbf{k} along the x axis the value of ω_d is $2\pi|\gamma|M_s$ in the circular-precession approximation.²¹ This can be understood intuitively as follows.²⁹

²⁹ C. Kittel (private communication). Also See Figs. 2.7 and 2.8 of Sparks (Ref. 20).

In Fig. 11(b), the values of m at half-wavelength intervals are represented by arrows. The vertical lines mark the positions at which m_x changes sign. Since the vertical region marked A resembles an infinite film, it is reasonable to expect that $\mathbf{h} \cong -4\pi m_x \hat{x}$ is a good approximation to the microwave demagnetization field for this spin wave. And $\mathbf{h} \sim -m_x \hat{x}$ implies that ω_d is proportional to M_s and is independent of \mathbf{k} . To see this we simply add the two equations in (4), which gives $\omega m^+ = (\omega_i + Dk^2)m^+ - |\gamma|Mh^+$, where $-\nabla^2$ has been replaced by k^2 . Setting

$$h^+ = -Cm_x + i(0) = -\frac{1}{2}C(m^+ + m^-)$$

and making the circular-precession approximation of neglecting m^- gives $\omega|\gamma| = H_i + Dk^2 + \frac{1}{2}CM_s$.

The analogous situation in a finite film with $k_z = 0$ is illustrated in Fig. 11(b). The magnitude of the demagnetization field of the region B (considered as a rectangular sample of constant magnetization \mathbf{m}) is less than $4\pi m_x$ because the surface poles, marked with $+$ and $-$, do not extend to infinity. From elementary electromagnetic theory, it is easy to show that the demagnetization field [determined by (3)] in the center of the rectangle B is

$$\mathbf{h} = -m_x(S/L)\hat{x} \int_{-S/2}^{S/2} dz \int_{-L/2}^{L/2} dy \frac{\lambda/4}{[(\frac{1}{4}\lambda)^2 + y^2 + z^2]^{3/2}}.$$

Neglecting z in the denominator (since $\lambda/4 \gg S/2$ for $\lambda \approx L$ and $L \gg S$), evaluating the integrals, and setting $\lambda \cong L$ gives $\mathbf{h} \sim -m_x(S/L)\hat{x}$. Thus ω_d is proportional to $M_s(S/L)$ for $k_f S \ll \pi$, in agreement with (44a).

From a similar argument we can see that $\omega_d \sim (S/L)^2 M_s$ for the higher-branch unpinned modes

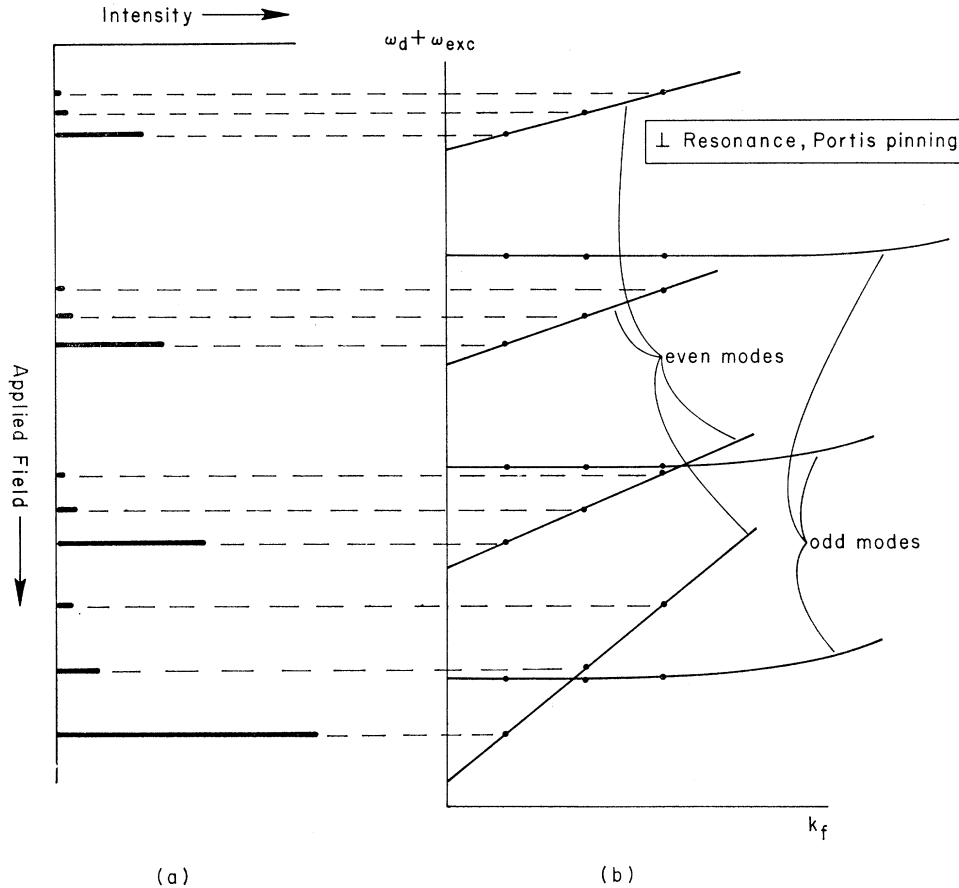


FIG. 13. Sketch of intensities (a) and dispersion relations (b) for Portis-pinned modes (in perpendicular resonance).

with $k_f \ll k_z$: Figure 11(c) represents $m^+ = \sin k_x x' \times \sin \pi z / S$ for the same value of k_x as in Fig. 11(d). The demagnetization field in the center of region C is clearly smaller than that in the center of region B because there are now positive and negative surface poles on each end of the region C+D. The nonzero contribution to the field at the center of region C depends on the difference between the distance d_+ to the positive poles and the distance d_- to the negative poles, which gives an extra power of (S/L) in ω_d ; thus $\omega_d \sim (S/L)^2 M_s$, in agreement with (44b). A similar argument shows that $\omega_d \sim (S/L)^2 M_s$ for the other higher-branch modes also. Since $S/L \ll 1$ for thin films, the demagnetization contribution ω_d to the frequency is much smaller for the higher-branch modes than for the main-branch modes.

Next consider the pinned modes. Figure 11(b) represents a mode with $m^+ \sim \cos \pi z / S$ (as well as one with $m^+(z) \sim 1$); therefore, $\omega_d \sim (S/L) M_s$ for this mode. Figure 11(c) represents a mode with $m^+ \sim \sin 2\pi z / S$; therefore, $\omega_d \sim (S/L)^2 M_s$ for this mode. The mode with $m^+ \sim \sin k_x x \cos 3\pi z / S$ is illustrated schematically in Fig. 11(d). The net positive value of the surface poles at the right of the region E+F+D is $\sim \frac{1}{3}$ of that of the

region B of Fig. 11(b). The net magnetization in the region E+F+D is also $\sim \frac{1}{3}$ of that in the region B; thus $\omega_d \sim (\frac{1}{3})^2 (S/L) M_s$. From this model, it is seen that when $k_f S \ll 1$, $\omega_d \sim (1/n_s)^2 (S/L) M_s$ for the even pinned modes, and $\omega_d \sim (S/L)^2 M_s$ for the odd pinned modes, in agreement with (29) and (44b). Note that the slope of ω_d as a function of k_f has the same n_s dependence as do the intensities I_n (see Sec. 8), e.g., I_n and slope $\sim 1/n_s^2$ for even pinned modes, I_n and slope = 0 for odd pinned modes, etc.

For the modes with very large values of k_x ($k_x \gg \pi/S$ and $k_x \gg k_z$), the region B (or C, D, etc.) is a thin plate, for which $\mathbf{h} = -4\pi m_x \hat{x}$. These modes therefore have $\omega_d = 2\pi |\gamma| M_s$ [in agreement with (44a) for $k_f \gg \pi/S$]. Thus the modes with large values of k_x would cluster near the top of the magnon manifold in perpendicular resonance if ω_{exc} were negligible. This argument also indicates that the spacing of the modes decreases as k_x increases (until Dk_x^2 becomes large).

Note that the demagnetization energy *decreases* with *decreasing inverse aspect ratio S/L*, while the exchange energy *increases* with *decreasing thickness S*. Thus, in the usual resonance experiment in which the frequency is fixed and the applied field H_{app} is varied, the higher-

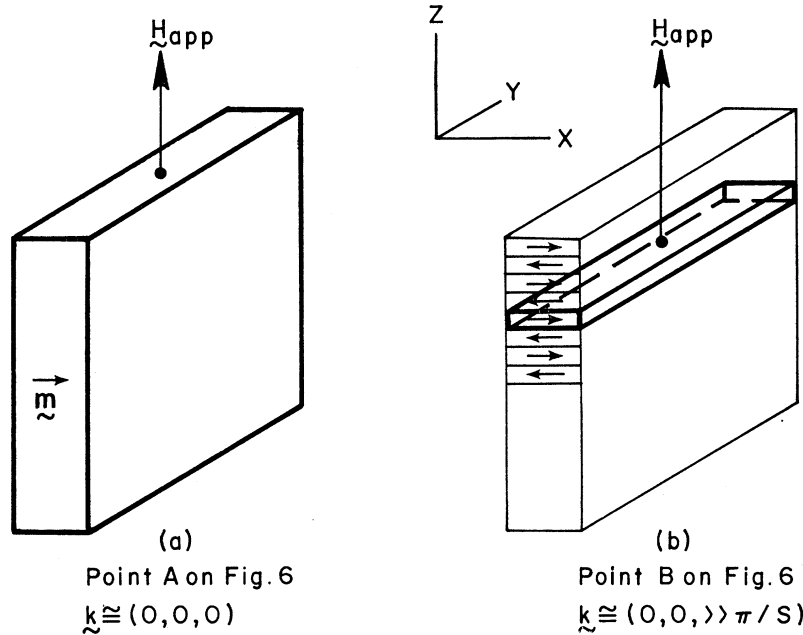


FIG. 14. Schematic illustration of m analogous to that of Fig. 11, but for parallel resonance: (a) for the main-resonance mode; (b) for a mode with k nearly parallel to the applied field $\hat{z}H_{app}$ and $k_z \gg \pi/S$.

branch modes become more widely spaced (larger differences in H_{app}) and the main-branch modes become more closely spaced as the film thickness is decreased.

From the same simple physical arguments used above to explain the theoretical results, it is easy to predict the effect of Portis pinning.⁵ Recall that if the saturation magnetization M_s varies across the film thickness as $M_s = M_0 - \Delta M f(z')$, where $\Delta M \ll M_0$ and $|f(z')| \leq 1$, the value of m^+ for the modes with $Dk^2 \lesssim 2\pi\Delta M$ is large only near the center of the film. In particular, Portis⁵ has shown that if M_s is parabolic in z' [i.e., $f(z') = (2z'/S)^2$], then $m^+(z')$ has the form of simple-harmonic-oscillator functions (rather than sinusoidal functions) for the low-order modes, as illustrated schematically in Fig. 12.

The first few even modes which are Portis⁵ pinned have relative intensities $1, \frac{1}{2}, \frac{3}{8}, \frac{5}{16},$ etc., and their exchange energies are proportional to $(n_s - \frac{1}{2})$. We have numbered the first mode as $n_s = 1$. With $n_s = 0$ for the first mode, the familiar result is $(n_s + \frac{1}{2})$. By using the fact that the slopes of ω_d as a function of k_f at $k_f = 0$ are proportional to the intensities, the dispersion relation can be sketched, as in Fig. 13. If $f(z')$ has a functional form different from $(2z'/S)^2$, the results are similar in general, but the intensities and slopes will differ from those of Portis.

The results for parallel resonance and oblique resonance (arbitrary θ_m) also can be obtained by the same type of physical model used above for perpendicular resonance. Very briefly, for the main-resonance mode [see Fig. 14(a) and point A on Fig. 6] the frequency is simply that of a thin film in parallel resonance, i.e., $\omega_d \cong 2\pi|\gamma|M_s$ in the circular-precession approximation. For k_z very large, the region marked by dark lines in

Fig. 14(b) resembles a thin film in perpendicular resonance, for which $\omega_d \cong 0$. For k_y very large, the region marked by dark lines in Fig. 15 resembles a thin film in parallel resonance; thus, $\omega_d \cong 2\pi|\gamma|M_s$. Figures 14(a) and 15 illustrate that $\omega_d \cong 2\pi|\gamma|M_s$ for all k_y when $k_z = 0$. See point C on Fig. 6.

In an infinite film in perpendicular resonance with no explicit surface pinning mechanism, the main-branch modes are nearly unpinned when $k_f < \pi/S$ and are nearly pinned when $k_f \gg \pi/S$, as discussed in Sec. 5. This result can be understood by considering Fig. 11(b). The field outside of the film along the z axis (with $x = 0$ in the center of region B) from the + and - sources shown in the figure drops off in a characteristic distance which is approximately equal to the spacing between the +'s and -'s, i.e., $\psi \sim \exp(-k_f z)$, roughly. Since ψ and $d\psi/dz$ are continuous at the surface, the slopes of ψ (and m) at the surface are small when $\frac{1}{2}\lambda \gg S$, and they are large when $\frac{1}{2}\lambda \ll S$. In other words, the surface spins are approximately unpinned for $k_f \ll \pi/S$ and are approximately pinned for $k_f \gg \pi/S$.

8. INTENSITIES OF MODES

The power I_n into the n th normal mode at resonance (i.e., the intensity of the mode) for a sample in a spatially constant microwave field $\mathbf{h}_{rf} = h_{rf}\hat{e}$ is

$$I_n = - \left(\int d\mathbf{r} \mathbf{h}_{rf} \cdot \frac{d\mathbf{M}_n}{dt} \right)_{\text{time av}} = g\omega_n h_{rf} c_n \int d\mathbf{r} m_{xn}, \quad (37')$$

where we have written the x component of \mathbf{M}_n as $c_n m_{xn}$. In this section, g is a generic constant (which is independent of c_n , m_{xn} , etc.). Since the energy density is proportional to $c_n^2 \tilde{m}_{xn}^2$, the power out of a mode with

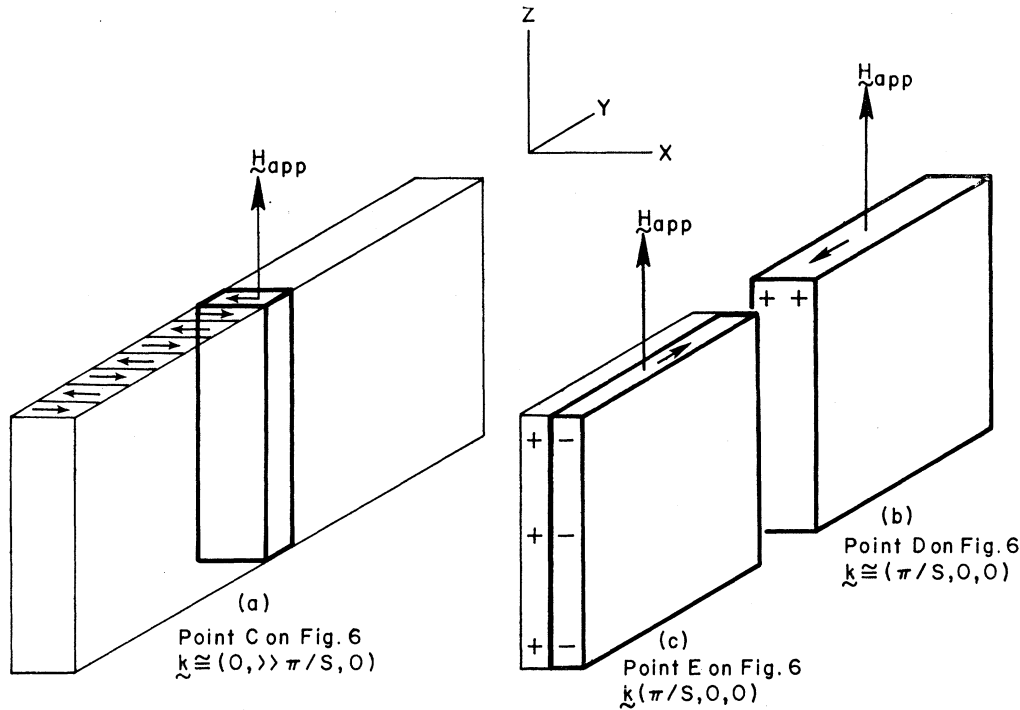


FIG. 15. Schematic illustration of m as in Fig. 14: (a) for a mode with k in the plane of the film and perpendicular to $\hat{z}H_{app}$ for the case of $k_y \gg \pi/S$; (b) and (c) effect of increasing k_x .

relaxation frequency $1/\tau_n$ and energy E_n is

$$\frac{E_n}{\tau_n} = g \frac{c_n^2}{\tau_n} \int d\mathbf{r} m_{xn}^2. \quad (38)$$

Equating (37') and (38) gives the equilibrium value of c_n :

$$c_n = g\tau_n \omega_n \left(h_{rf} \int d\mathbf{r} m_{xn} / \int d\mathbf{r} m_{xn}^2 \right).$$

With this value of c_n , (37') gives

$$I_n = gh_{rf}^2 \frac{\omega_n^2}{\Delta H_n} \left| \int d\mathbf{r} m_{xn} \right|^2 / \int d\mathbf{r} m_{xn}^2 \quad (39)$$

for the intensity of the n th mode, where $\Delta H_n = g/\tau_n$ is the linewidth of the n th mode. This result shows that in the usual experiment at fixed frequency (and varying H_{app}), the intensities of the modes are proportional to $|\int d\mathbf{r} m_{xn}|^2 / \Delta H_n$, when m_{xn} is normalized as

$$\int d\mathbf{r} m_{xn}^2 = 1.$$

Consider a rectangular film. For the pinned even modes, (39) gives

$$I_n = \frac{g}{n_s^2 n_w^2 n_L^2 \Delta H_n} \quad \text{even pinned modes} \quad (40)$$

and for the unpinned even modes on the main branch

(39) gives

$$I_n = \frac{g}{n_w^2 n_L^2 \Delta H_n}$$

even unpinned main-branch modes. (41)

The intensities of all odd modes and of the unpinned higher-branch modes are zero since $\int d\mathbf{r} m_{xn} = 0$ for these modes.

For a circular film in a constant microwave field in perpendicular resonance, $I_n = 0$ for all modes with azimuthal number $l \neq 0$ in (49). For $l = 0$, $m_x = J_0(k_\rho \rho) \times \cos(k_z z - \frac{1}{2} \eta_z \pi)$. Using

$$\int_0^{r_0} d\rho \rho J_0^2(k_\rho \rho) = \frac{1}{2} r_0^2 [J_0^2(k_\rho r_0) + J_1^2(k_\rho r_0)]$$

and

$$\int_0^{r_0} d\rho \rho J_0(k_\rho \rho) = \frac{1}{k_\rho} J_1(k_\rho r_0)$$

in (39) gives

$$I_n = g \frac{1}{k_\rho^2 \Delta H_n} \left(\frac{J_1^2(k_\rho r_0)}{J_0^2(k_\rho r_0) + J_1^2(k_\rho r_0)} \right). \quad (42)$$

Since we are considering only modes which are pinned

at $r=r_0$, $J_0(k_\rho r_0)=0$, and (42) reduces to

$$I_n = \frac{g}{k_\rho^2 \Delta H_n} \quad \text{main-branch modes with } l=0.$$

The approximate results for I_n given above should be quite good for the higher-order modes in a given series, the integral of m_{xn} in (39) being controlled by the number of half-sine-waves in m_{xn} since pairs of positive and negative half-sine-waves integrate to zero. However, the intensities of the first few modes in a given series may differ considerably from the theoretical values since the integral of m_{xn} depends more strongly on the detailed shape of m_{xn} than does ω_n : A difference ϵ in the trial function \tilde{m}_n^+ from the true function m_n^+ gives an error in the frequency which is proportional to ϵ^2 but the error in I_n is proportional to ϵ .

9. EFFECT OF PINNING ON FREQUENCIES AND INTENSITIES

The effect of pinning at the small edges of film was considered in Secs. 4 and 6. We now consider the pinning at the large faces ($z'=\pm\frac{1}{2}S$). The frequencies and intensities of pinned and unpinned exchange modes are quite different.⁴ However, the frequencies and intensities of magnetostatic modes are relatively insensitive to the amount of surface spin pinning, as discussed elsewhere.²⁴ This insensitivity can be understood intuitively as follows.

First, it is easy to see that pinned sine waves are not solutions to (6), or to (2) and (3), when the exchange constant $\Lambda=0$. This can be proved by direct substitution and can be understood intuitively as follows: Consider, for example, a perpendicular-resonance mode with $k_f S \ll 1$. The argument in the last paragraph of Sec. 7 shows that $d\mathbf{h}/dz \cong 0$ at $z=\pm\frac{1}{2}S$. When $\Lambda=0$, \mathbf{m} is proportional to \mathbf{h} ; thus $d\mathbf{m}/dz=0$ at $z=\pm\frac{1}{2}S$, and the mode is not pinned. This is an example of a general result that imposing a pinning condition, such as $\mathbf{m}=0$, on the magnetostatic-mode problem with $\Lambda=0$ over-determines the boundary conditions at $z'=\pm\frac{1}{2}S$, and no solution exists. In this case it is necessary to include the exchange interaction even though $Dk^2 \ll \omega a$. (Mathematically, the exchange term is a singular perturbation.) Then the solutions to (2) and (3) in an infinite film are linear combinations of terms containing three wave vectors,¹⁴ in contrast to the exchange case or the pure magnetostatic case ($\Lambda=0$ and no explicit pinning) for which only one wave vector is required. For a given \mathbf{k}_f , the three values of $k_{z'}^2$ are easily found by substituting $m_x, m_y \sim \cos k_{z'} z'$ into (2) and (3). The result is that the three values of $k_{z'}^2$ are simply the roots of the dispersion relation $k^2 \Omega^2 = k^2 (\Omega_H + \tilde{\Lambda} k^2) (\Omega_H + \tilde{\Lambda} k^2 + \sin^2 \theta_k)$, where $\Omega \equiv \omega/4\pi |\gamma| M_s$, $\Omega_H \equiv H_i/4\pi M_s$, $\tilde{\Lambda} \equiv \Lambda/4\pi$, and $\sin^2 \theta_k = (k_x^2 + k_y^2)/k^2$, which is obtained by squaring both sides of (30) and multiplying by k^2 .

In perpendicular resonance, $k_{z'}=k_z$ and $k_f^2=k_x^2+k_y^2$, where z' and z are always the axes normal to the plane of the film and along \mathbf{H}_i , respectively. In parallel resonance, $k_{z'}=k_x$, $k_{y'}=k_y$, and $k_{x'}=k_z$. The resulting values of k_z for magnetostatic modes in perpendicular resonance are k_{ms} , k_E , and ik_{ngl} , where

$$k_{ms}^2 \cong k_f^2 (\Omega_H^2 + \Omega_H - \Omega^2) (\Omega^2 - \Omega_H^2)^{-1}, \quad (43a)$$

$$k_E = \pm [(\Omega - \Omega_H)/\tilde{\Lambda}]^{1/2}, \quad ik_{ngl} = \pm i [(\Omega + \Omega_H)/\tilde{\Lambda}]^{1/2}. \quad (43b)$$

The first wave vector k_{ms} is the usual magnetostatic-mode wave vector.¹² Solving (43a) for Ω gives $\Omega \cong [\Omega_H (\Omega_H + \sin^2 \theta_k)]^{1/2} \equiv \Omega_{ms}$, which is just the frequency of a pure magnetostatic mode.¹² Since $\Omega = \Omega_H + \tilde{\Lambda} k^2$ for an exchange mode, (43b) shows that k_E is the wave vector for an exchange wave which has the same frequency as the magnetostatic wave. The frequency of a wave $f(\mathbf{r})$ will be defined as the precessional frequency for a magnetization having $\mathbf{m} \sim f(\mathbf{r})$, the Zeeman frequency being positive and the exchange frequency being positive for oscillating waves [negative $\alpha \equiv (d^2 m_x/dz'^2)/m_x$] or negative for decaying waves (positive α). The wave frequency Ω_E for the k_E wave is $\Omega_E = +\Omega_{ms}$, and that of the ik_{ngl} wave is $\Omega_{ngl} = -\Omega_{ms}$. The k_{ms} and k_E waves can be admixed freely to satisfy the surface pinning conditions (such as $\mathbf{m}=0$ or $d\mathbf{m}/dz'=0$, for example) since the wave frequencies are the same. The decaying ik_{ngl} wave is far off frequency ($\Omega = -\Omega_{ms} \neq +\Omega_{ms}$) since α is positive, and its amplitude is negligible.

Since $\Lambda(\pi/S)^2 \ll 1$ for magnetostatic modes, the k_E wave must have many oscillations in order to make its frequency $\Omega_H + \Lambda k_E^2$ equal to the magnetostatic-wave frequency Ω_{ms} . Thus the intensity is controlled by the term $\cos k_{ms} z$ since $\cos k_E z$ integrates to zero approximately. In other words, the intensities of the magnetostatic modes are the same as those of the pure magnetostatic modes (having $\Lambda=0$ and no explicit pinning). The field \mathbf{h} is essentially unaffected by the addition of the $\cos k_E z$ wave since the source $(\nabla \cdot \mathbf{m})$ of \mathbf{h} oscillates rapidly, thereby integrating to zero approximately. Thus, ψ and $d\psi/dz$ are still continuous at $z=\pm\frac{1}{2}S$ when the k_E wave is added.

Next consider parallel resonance. For surface modes with $k_z=0$, the values of $k_x \equiv k_{z'}$, obtained from the solution of the dispersion relation, are $k_x = ik_{su}$, k_+ , and k_- , where $k_{su} = \pm k_y$ and $\Lambda k_\pm^2 = -(\Omega_H + \frac{1}{2}) \pm (\frac{1}{4} + \Omega^2)^{1/2}$. The frequency Ω_{su} of the ik_{su} wave is simply the frequency of the pure magnetostatic surface wave.¹¹ The frequencies of the k_\pm waves are $\Omega_\pm = \pm \Omega_{su}$.³⁰ The decaying k_- wave is off frequency, and its amplitude is negligible. The oscillating k_+ wave has the same fre-

³⁰ The following results in this and the next paragraph were obtained by analogy with the results for perpendicular resonance, except for the values of k_x and Ω , which were calculated directly. See Ref. 24.

quency as the surface wave, and a linear combination of these two waves is chosen to satisfy the surface pinning conditions. As in perpendicular resonance, the intensity is controlled by the magnetostatic wave since the rapidly oscillating k_+ wave integrates to zero approximately.

For the bulk modes with $k_y=0$ in parallel resonance, solving the dispersion relation for k_x gives $\Lambda k_{(\pm)}^2 = -\Omega_H - \frac{1}{2} \pm [(\Omega_H + \frac{1}{2}) - (\Omega_{top}^2 - \Omega^2)]^{1/2}$ for the two extra waves, both of which are decaying in the present case. Here $\Omega_{top}^2 \equiv \Omega_H^2 + \Omega_H$. The third wave vector k_{ms} is just the Damon and Eshbach¹¹ bulk-mode wave vector. The three frequencies are Ω_{ms} , $\Omega_{dec} = \Omega_{ms}$, and $\Omega_{ngb} = -\Omega_{ms}$, where Ω_{ms} is the Damon and Eshbach frequency, $ik_{dec} \equiv k_{(+)}$, and $ik_{ngb} \equiv k_{(-)}$. The ik_{ngb} wave is off frequency, and its amplitude is negligible. A linear combination of the degenerate k_{ms} and ik_{dec} waves is chosen to satisfy the surface pinning conditions. The second (ik_{dec}) wave is decaying, in contrast to the results of the previous two cases, because the frequency must be lowered from Ω_{top} to Ω_{ms} and a positive α (decaying wave) lowers the frequency. This ik_{dec} wave changes \mathbf{m} only very near the surfaces, where it rounds off \mathbf{m} to zero at $x = \pm \frac{1}{2}S$.

Several experimental results can be explained in terms of these theoretical results. Sparks and co-workers² observed that the higher-branch magnetostatic modes in a 12.4- μ -thick YIG film had very small intensities (roughly 700 times smaller than that of the main-resonance mode). It is likely that the surface spins were pinned since a surface roughness as small as $\sim 200 \text{ \AA}$ should pin the spins,¹⁷ for example. Single-sine-wave pinned modes would have large intensities [$\sim \frac{1}{9}$ that of the main resonance, as in Fig. 5(a)] in contrast to the small observed intensities. The two-wave solutions discussed above should have small intensities, in agreement with the experimental results. Although the results above indicate that pinning the magnetostatic modes at a shape surface should not give rise to the large intensities and nonzero slopes of ω versus k_f of the single-wave pinned modes, the pinned exchange modes and mixed modes are expected to have large intensities and nonzero slopes, as in Figs. 5 and 13.

The experimental results² also indicated that for thinner films (for which the higher-branch modes were exchange modes) the higher-branch modes had large intensities, as expected for pinned exchange modes. Later experiments by Besser¹⁵ indicate that some of the YIG films presently available may be of such high quality that the exchange modes are not pinned. The theoretical results also explain the fact that surface modes have been observed^{16,31} under conditions for which the surface spins are expected to be pinned.¹⁷ It might have been expected that making $\mathbf{m}=0$ at the

surface would have essentially eliminated the surface modes, but the two-mode results above indicate that this is not the case. It is reasonable to expect that the result for other geometries, such as spheroids, should be similar. For example, pinning the surface spins in a spherical sample should not make large changes in the frequencies or intensities of the observed magnetostatic modes,^{6,9} which have large amplitudes at the surfaces in general in the absence of explicit pinning.

The results indicate that the basic idea of Benson and Mills¹⁸ of a two-wave solution is essentially correct for magnetostatic waves. (Their "rounder function" $1 - \alpha z^2$ can be replaced by an exponential wave, giving a two-wave solution.) However, the added wave is an oscillating wave, rather than a decaying one, in some cases as discussed above.

Several conclusions of Wolfram and De Wames,¹⁴ based on incorrect generalizations of computer solutions for m_x and ω for several specific values of $k_f S$, Ω_H , etc., contradict the present results. The k_E or k_+ wave, not the ik_{ngl} or k_- wave, is the important one for satisfying the boundary conditions, and the amount of the k_E or k_+ wave in \mathbf{m} is large away from the crossovers in general. In their semi-infinite-medium calculation of the lifetimes of surface modes, their solution satisfies the surface conditions only at certain isolated instances of time since a travelling wave $m_x \sim \exp(ik_x x)$ (with implicit $\exp i\omega t$ time dependence) cannot satisfy their pinning condition $dm_x/dx = 0$ at $x=0$ for all times. It is misleading to consider \mathbf{m} as an admixture of bulk and surface waves simply because one k_x is imaginary and another is real. For example, the ik_{dec} wave above rounds off \mathbf{m} to zero at the surface, while surface waves have large values of \mathbf{m} at the surface.

10. SUMMARY OF THEORETICAL RESULTS

The result of the variational calculation for the frequencies of the ferromagnetic normal modes of a thin film is

$$\frac{\omega}{|\gamma|} = [(\langle H_i \rangle + Dk^2)(\langle H_i \rangle + Dk^2 + 2\bar{\omega}_d)]^{1/2}, \quad (43c)$$

where $H_i \cong H_{app} - H_D$ [Sec. 6] and $\bar{\omega}_d \equiv \omega_d / |\gamma|$. The results for ω_d in rectangular films are as follows: For the unpinned modes with arbitrary θ_m , ω_d is given by (26) and (27) for the main-branch and higher-branch modes, respectively [Sec. 4]. For perpendicular resonance, $\theta_m \equiv 0$, $x' = x$, $y' = y$, and $z' = z$; thus (26) and (27) give

$$\omega_{d1} = 2\pi |\gamma| M_s \left[1 - \frac{1}{k_f S} (1 - e^{-k_f S}) \right],$$

main branch, unpinned (44a)

$$\omega_{d1} = 2\pi |\gamma| M_s \sin^2 \theta_k,$$

higher branches, unpinned (44b)

³¹ F. A. Pizzarello and J. H. Collins, in Fifteenth Annual Conference on Magnetism and Magnetic Materials, Philadelphia, 1969 (unpublished); J. Appl. Phys. (to be published).

where $\sin^2\theta_k = k_f^2/k^2$. For parallel resonance, $\theta_m = 90^\circ$, and (26) and (27) give

$$\omega_{d||} = 2\pi|\gamma|M_s - 2\pi|\gamma|M_s \cos^2\phi' \left[1 - \frac{1}{k_f S} (1 - e^{-k_f S}) \right],$$

main branch, unpinned (45a)

$$\omega_{d||} = 2\pi|\gamma|M_s \sin^2\theta_k,$$

higher branches, unpinned (45b)

where

$$\sin^2\theta_k = (k_y^2 + k_z^2)/k^2$$

and

$$\cos^2\phi' = k_x^2/(k_x^2 + k_y^2).$$

For single-wave-vector pinned odd modes, ω_d is given by (27) [or (44b) or (45b) for $\theta_m = 0$ or 90° , respectively], and for pinned even modes, with $k_f S \ll \pi$, ω_d is given by (see Sec. 4)

$$\omega_d = (8/\pi)|\gamma|M_s k_f S / n_s^2. \quad (29a)$$

For a circular film in parallel resonance with $l=0$ (no azimuthal nodes in m^+),³² it is shown in the Appendix that Eqs. (44) are valid if k_f is replaced by the radial wave vector k_p and ω_d for the main-resonance mode is multiplied by $[1 - (2\tau_n/k_f S)]/\tau_n$, where τ_n is the factor in the bracket in (44a). For the usual case of $k_f S \ll 1$, this correction factor for the main-resonance mode in a circular film is approximately equal to 0.67. For a rectangular film, the values of k_f are

$$k_f = (\pi/L)[n_L^2 + (L^2/W^2)n_W^2]^{1/2}, \quad (46)$$

where $n_L, n_W = 1, 2, 3, \dots$. For a circular film, the values of k_p for $l=0$ are

$$k_p r_0 / \pi = 0.76, 1.76, 2.75, \dots (n - 0.25), \dots, \quad (47)$$

which are the roots of $J_0(k_p r_0) = 0$, with r_0 as the radius of the film.

The essential features of these theoretical results, most of which are illustrated in Figs. 3-9 and 13, are the following: (a) The modes can be conveniently divided into branches, which correspond to different values of k_z . The different modes on a given branch have different values of k_f (Sec. 4). (b) All of the low-order modes (small k_f) on a given branch have approximately the same value of $\omega_{\text{exc}} \cong Dk_z^2$, which is proportional to n_s^2/S^2 and is independent of F , where F is a face dimension such as the radius or length. (c) The modes on a given branch have different amounts of demagnetization energy $\hbar|\gamma|\omega_d$ in general, as seen in Figs. 3-9. (d) The slope of ω as a function of k_f at the origin is nonzero for the main branch, which implies that $\omega_d \sim S/F$. (e) The modes on the main branch become more closely spaced in frequency as k_f increases, corresponding to the flattening of ω_d as a function of k_f , as seen in Figs. 3-9.

³² The case of $l \neq 0$ is considered elsewhere: M. Sparks, Solid State Commun. (to be published).

For single-wave-vector *unpinned modes*: (f) The higher branches have zero slope at the origin, which implies that $\omega_d \sim S^2/F^2$ for small values of k_f . Thus the low-order higher-branch modes are much more closely spaced in frequency than are the low-order main-branch modes. (g) The intensity of the main-resonance mode is large, and the intensities of the other main-branch modes decrease as k_f increases. The intensities of all higher-branch modes with $k_f \ll k_z$ are theoretically approximately zero.

For single-wave-vector *pinned modes*: (h) The slope of ω_d was a function of k_f and the values of I_n are largest for the main branch, and they decrease rather slowly for the higher branches for the pinned even modes. The values of I_n and the slope of ω_d at the origin are much smaller ($\omega_d \sim S^2/F^2$ and $I_n = 0$) for the pinned odd modes on the higher branches. These formal results are for a single wave vector m^+ . The frequencies and intensities of magnetostatic modes (but not exchange modes) are expected to be relatively independent of surface-spin pinning; the results for $k_f \ll k_z$ (or for $k_f \gg k_z$) are approximately the same as the single-wave-vector results for unpinned (or for pinned) modes. See Sec. 9.

The effects of an inhomogeneity in H_i across z' are discussed briefly in Sec. 6 and in more detail in Paper IV. The effects of the inhomogeneity in H_i along r_0 (or W and L) are difficult to calculate accurately, but the following results may be useful as a rough estimate of the effects on $\langle H_i \rangle$ and $\bar{\omega}_d \equiv \omega_d / |\gamma|$ for the magnetostatic modes. The value of $\langle H_i \rangle$ in (43c) can be written as

$$\langle H_i \rangle = H_{\text{app}} - 4\pi M_s + \langle \delta H_D \rangle,$$

where

$$\langle \delta H_D \rangle = g(S/2r_0)(4\pi M_s). \quad (36''''')$$

For the main branch, g increases from a value slightly larger than 1 for the main-resonance mode to a value of $g \cong 7/4$ for the high-order modes. For the low-order higher-branch magnetostatic modes, $g \cong 1$.

The approximate value of $\delta\bar{\omega}_d$ for the main-resonance mode can be obtained by the method of Sec. 6, or with somewhat less accuracy from the relation

$$\delta\bar{\omega}_d \cong (2S/r_0)\bar{\omega}_d(r_0). \quad (36''''')$$

For the high-order modes and for the low-order higher-branch modes, $\delta\bar{\omega}_d \cong 0$. These two terms $\langle \delta H_D \rangle$ and $\delta\bar{\omega}_d$ increase the width of the normal-mode manifold, increase the spacings of the low-order main-branch modes, and increase the spacing between the main-resonance mode and the highest-field modes.

ACKNOWLEDGMENTS

Stimulating conversations with P. Besser, J. H. Collins, R. E. De Wames, D. L. Mills, C. Newkirk, B. R. Tittmann, and T. Wolfram are gratefully acknowledged. T. Wolfram made valuable suggestions for improving the manuscript.

APPENDIX: FREQUENCIES FOR CIRCULAR FILMS

It can be shown²⁴ that the exact solutions of the Walker potential problem⁷ for ψ inside of an infinite film for perpendicular resonance in circular-cylindrical coordinates is

$$\psi = J_n(k_\rho \rho) \cos(k_z z - \frac{1}{2} \eta_z \pi) e^{-in\phi}, \quad (48)$$

where J_n is the Bessel function of integer order n and $\eta_z = 0$ or 1 as in (15). As the trial function for a finite disk-shaped film we choose the m^+ obtained from (48) by the relation $m^+ = \kappa^- \partial^+ \psi$, where κ^- is a constant and ∂^+ is defined under (6). By using

$$\partial^+ e^{-in\phi} = (n/\rho) e^{-i(n-1)\phi}, \quad \partial^+ J_n(k_\rho \rho) = k_\rho e^{i\phi} J_n'(k_\rho \rho),$$

where the prime denotes the derivative with respect to the argument, and setting $l = n - 1$, it is easy to show that

$$m^+ = \kappa^- k_\rho \exp(-il\phi) J_l(k_\rho \rho) \cos(k_z z - \frac{1}{2} \eta_z \pi). \quad (49)$$

Substituting (49) into (14) and using $\exp(i\mathbf{q} \cdot \mathbf{r}) = \exp(iq_\rho \rho \cos\phi + iq_z z)$ and

$$\int_0^{2\pi} d\phi e^{iq_\rho \rho \cos\phi} e^{-il\phi} = 2\pi i^l J_l(q_\rho \rho)$$

gives

$$\begin{aligned} \omega_{dC} &= \frac{|\gamma| M_s}{2\pi} \int d\mathbf{q} \frac{q^2}{q^2} \left| \int_{-S/2}^{S/2} dz \cos(k_z z - \frac{1}{2} \eta_z \pi) e^{iq_z z} \right|^2 \\ &\times \left| \int_0^{r_0} d\rho \rho J_l(q_\rho \rho) J_l(k_\rho \rho) \right|^2 \left(\int_0^{r_0} d\rho \rho J_l^2(k_\rho \rho) \right. \\ &\quad \left. \times \int_{-S/2}^{S/2} dz \cos^2(k_z z - \frac{1}{2} \eta_z \pi) \right)^{-1}. \quad (50) \end{aligned}$$

To simplify the arithmetic, first consider the case of no azimuthal nodes in \mathbf{m} , i.e., $l = 0$; these are the only modes which couple to a spatially constant microwave field. For the first case of $k_z \ll \pi/S$ and $k_\rho r_0 \gg 1$ we use the approximations

$$J_0(\xi) = \cos(\xi - \frac{1}{4}\pi) / (\frac{1}{2}\pi\xi)^{1/2} \quad \text{for } \xi \gtrsim 2\pi$$

and

$$\int_0^{r_0} d\rho \cos k_\rho \rho \cos q_\rho \rho \cong \frac{\sin(q_\rho - k_\rho)r_0}{2(q_\rho - k_\rho)} \quad \text{for } k_\rho r_0 \gg 1$$

to obtain

$$\left| \int_0^{r_0} d\rho \rho J_0(k_\rho \rho) J_0(q_\rho \rho) \right|^2 \cong \frac{r_0^2}{\pi^2 k_\rho^2} \left(\frac{\sin(q_\rho - k_\rho)r_0}{(q_\rho - k_\rho)r_0} \right)^2. \quad (51)$$

Using (51), (23), and

$$\int_0^{r_0} d\rho \rho J_0^2(k_\rho \rho) = \frac{1}{2} r_0^2 [J_0^2(k_\rho r_0) + J_1^2(k_\rho r_0)] \cong \frac{r_0}{\pi k_\rho}$$

(for $k_\rho r_0 \gg 1$) in (50) gives

$$\omega_{dC} = \frac{|\gamma| M_s r_0 S}{2\pi^2 k_\rho} \int_{Q_a} d\mathbf{q} \frac{q_\rho^2 \sin^2 \frac{1}{2} q_z S}{q^2 (\frac{1}{2} q_z S)^2}, \quad (52)$$

where Q_a is the volume defined by $|q_\rho - k_\rho| < \pi/2r_0$. Approximating q_ρ^2 by its average k_ρ^2 over Q_a and using $d\mathbf{q} \cong 2\pi k_\rho (\pi/r_0) dq_z$ in (52) gives

$$\begin{aligned} \omega_{dC} &= |\gamma| M_s k_\rho^2 S \int_{-\infty}^{\infty} dq_z \frac{1}{q_z^2 + k_\rho^2} \frac{\sin^2 \frac{1}{2} q_z S}{(\frac{1}{2} q_z S)^2} \\ &= 2\pi |\gamma| M_s \left[1 - \frac{1}{k_\rho S} (1 - e^{-k_\rho S}) \right] \quad (53) \end{aligned}$$

for this case of $k_z \ll \pi/S$ and $k_\rho r_0 \gg 1$.

We now show that (53) is a fairly good approximation even for the lowest-order mode which is pinned at $r = r_0$, i.e., for $k_\rho r_0 = 2.4$, where 2.4 is the first zero of J_0 . When $q_\rho = 0$, the value of the ρ integral in (50) is

$$\left| \int_0^{r_0} d\rho \rho J_0(k_\rho \rho) \right|^2 = \frac{r_0^2}{k_\rho^2} J_1^2(k_\rho r_0) = \frac{J_1^2(2.4)}{(2.4)^2} r_0^4.$$

Since $(k_\rho \rho)^{1/2} J_0(k_\rho \rho)$ has no zeros between $\rho = 0$ and $\rho = r_0$ and the function $(q_\rho \rho)^{1/2} J_0(q_\rho \rho)$ has many oscillations between $\rho = 0$ and $\rho = r_0$ when $q_\rho \gg 2.4/r_0$, the ρ integrand in (50) is a rapidly decreasing function of q_ρ when $q > 2.4/r_0$. Thus

$$\begin{aligned} \left| \int_0^{r_0} d\rho \rho J_0(k_\rho \rho) J_0(q_\rho \rho) \right|^2 &\cong \frac{J_1^2(2.4)}{(2.4)^2} r_0^4 \quad \text{for } q_\rho r_0 < 2.4 \\ &\cong 0 \quad \text{for } q_\rho r_0 > 2.4. \end{aligned}$$

With this result and

$$\int_0^{r_0} d\rho \rho J_0^2\left(\frac{2.4\rho}{r_0}\right) = \frac{1}{2} r_0^2 J_1^2(2.4),$$

(50) gives

$$\omega_{dC} = \frac{|\gamma| M_s S}{\pi k_\rho^2} \int_{Q_b} d\mathbf{q} \frac{q_\rho^2 \sin^2 \frac{1}{2} q_z S}{q^2 (\frac{1}{2} q_z S)^2},$$

where Q_b is the volume defined by $q_\rho < 2.4/r_0$. Evaluating the integrals gives

$$\omega_{dC} = 2\pi |\gamma| M_s (1 - 2\tau_n/f) \quad (54)$$

for the main-resonance mode in a circular film. Here $f \equiv k_\rho S$ and $\tau_n = 1 - f^{-1} [1 - \exp(-f)]$. For the usual

case of $f \ll 1$ for the main-resonance mode, the value of ω_d from (54) is ~ 0.67 times as large as that from (53).

The exact solution²⁴ for the infinite-film problem in circular-cylindrical coordinates for no exchange ($D=0$) is given by (30) with

$$\sin^2 \theta_k = k_\rho^2 / (k_\rho^2 + k_z^2), \quad (55)$$

where k_z is given by (32) (or the corresponding result for odd modes) with k_f replaced by k_ρ . For pinning at the edges of the film ($r_0=0$), the values of k_ρ are given by the

roots of the equation

$$J_l(k_\rho r_0) = 0.$$

Thus, the values of k_ρ are different for modes having different values of azimuthal number l . For $l=0$, this gives the values $k_\rho = 0.76\pi/r_0, 1.76\pi/r_0, \dots$ listed in Sec. 5. Considering the other values of l offers an explanation²⁴ of the observation of Dillon⁶ that the first, second, \dots , fifth modes in a sample containing a small imperfection on its edge contained one, two, \dots , five lines, respectively.

Ferromagnetic Resonance in Thin Films. II. Theory of Linewidths

M. SPARKS*

Science Center, North American Rockwell Corporation, Thousand Oaks, California 91360

(Received 28 July 1969)

The ferromagnetic-resonance linewidth ΔH from two-magnon processes in thin films is calculated. The results are quite different from those in spheroidal samples in general, since both the densities of states and the scattering Hamiltonians are different. It is shown that it should be possible to choose the radius and thickness of a ferromagnetic insulator thin film in such a way to make the frequency of the main-resonance mode lie well below the frequencies of all other magnetic modes. The resulting small ΔH 's make the films important for studying ferromagnetic-resonance linewidths and afford a useful low-loss system. For scattering centers (such as pits and scratches on the surface of the sample or etch pits extending through the sample thickness) which are smaller than the film thickness, the results are similar to those of Sparks, Loudon, and Kittel (SLK) for a spherical sample. A modification of the SLK result is given which removes the divergence in ΔH at parallel resonance and also makes ΔH go smoothly to zero at perpendicular resonance. For scattering centers which are larger than the film thickness, ΔH has a rather large maximum at an angle approximately one-half way between perpendicular and parallel resonance, in contrast to the small-scattering-center result of a maximum at parallel resonance. In addition to these results for the main-resonance mode, it is shown that the mode-number- n dependence of the two-magnon linewidths of exchange modes (having negligible microwave demagnetization energy) varies in a rather complicated way from $\Delta H \sim n^3$ for small n to $\Delta H \sim n^2$ and $\Delta H \sim n$ for intermediate n to $\Delta H \sim n^0$ for large n .

1. INTRODUCTION

RECENTLY, Mee and co-workers¹ have succeeded in growing single-crystal thin films of yttrium iron garnet (YIG) ranging in thickness from ~ 0.5 to 40μ . Since bulk films can be ground to a thickness as small as 15μ , single-crystal YIG films with any thickness greater than $\sim 0.5 \mu$ are now available. These films promise to become important ferromagnetic-resonance systems for the following reasons: It is possible to choose the thickness S and the radius R of a film in such a way that there are no magnetic modes degenerate with the main-resonance mode of the film. The resulting small linewidths ΔH should be important for applications requiring low-loss materials, and linewidth mechanisms

which were heretofore masked by the large two-magnon process could be investigated in resonance experiments, as discussed elsewhere.²

The density of degenerate states can be controlled experimentally over a vast range from zero to very large values. It may be possible to study such interesting effects as mode clamping,³ comparison of the relaxation frequencies of wave packets and standing waves, linewidths of surface waves on the YIG-substrate interface and on the YIG-air interface, interaction of magnetic and acoustic surface waves, effect of the nonzero relaxation frequencies of the degenerate modes, and comparison of golden-rule relaxation frequencies with normal-mode relaxation frequencies.

The ferromagnetic-resonance linewidth arising from two-magnon scattering in bulk-type samples (e.g., spheroids and thick disks) has been considered by

* Present address: The RAND Corp., Santa Monica, Calif., 90406.

¹ J. E. Mee, J. L. Archer, R. H. Meade, and T. N. Hamilton, *Appl. Phys. Letters* **10**, 289 (1967); J. E. Mee, *IEEE Trans. MAG-3*, 190 (1967).

² M. Sparks, *Phys. Rev. Letters* **22**, 1310 (1969).

³ M. Sparks, *Quart. Appl. Math* (to be published).